ACS Pharmacology & Translational Science

Open Access

pubs.acs.org/ptsci

Article

A Highly Potent, Orally Bioavailable Pyrazole-Derived Cannabinoid CB2 Receptor- Selective Full Agonist for *In Vivo* Studies

Andrea Chicca, Daniel Bátora, Christoph Ullmer, Antonello Caruso, Sabine Grüner, Jürgen Fingerle, Thomas Hartung, Roland Degen, Matthias Müller, Uwe Grether, Pal Pacher,* and Jürg Gertsch*

Cite This: *ACS Pharmacol. Transl. Sci.* 2024, 7, 2424−2438

Read Online

ACCESS | Metrics & More | Article Recommendations | Supporting Information

ABSTRACT: The cannabinoid CB2 receptor (CB2R) is a potential therapeutic target for distinct forms of tissue injury and inflammatory diseases. To thoroughly investigate the role of CB2R in pathophysiological conditions and for target validation *in vivo*, optimal pharmacological tool compounds are essential. Despite the sizable progress in the generation of potent and selective CB2R ligands, pharmacokinetic parameters are often neglected for *in vivo* studies. Here, we report the generation and characterization of a tetra-substituted pyrazole CB2R full agonist named RNB-61 with high potency (K_i 0.13−1.81 nM, depending on species) and a peripherally restricted action due to *P*-glycoprotein-mediated efflux from the brain. ^{3}H and ^{14}C labeled RNB-61 showed apparent K_d values of <4 nM toward human CB2R in both cell and tissue experiments. The 6,800-fold selectivity over CB1 receptors and negligible off-targets *in vitro*, combined with high oral bioavailability and suitable systemic pharmacokinetic (PK) properties, prompted the assessment of RNB-61 in a mouse ischemia-reperfusion model of acute kidney injury (AKI) and in a rat model of chronic kidney injury/inflammation and fibrosis (CKI) induced by unilateral ureteral obstruction. RNB-61 exerted dose-dependent nephroprotective and/or antifibrotic effects in the AKI/CKI models. Thus, RNB-61 is an optimal CB2R tool compound for preclinical *in vivo* studies with superior biophysical and PK properties over generally used CB2R ligands.

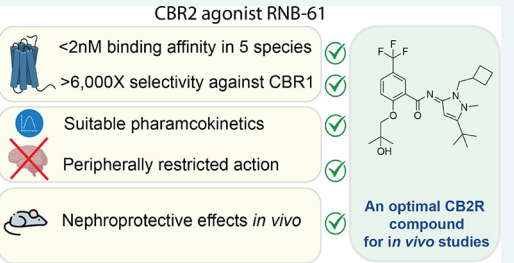

KEYWORDS: *cannabinoid 2 receptors, inflammation, drug development, pharmacokinetics, in vivo studies*

Cannabinoid CB1 receptors (CB1Rs) are expressed both in the central nervous system and peripherally and are responsible for the neuropharmacological effects of psychoactive cannabinoids like Δ9-THC.[1,2] In contrast, CB2 receptors (CB2Rs) are expressed primarily in the immune system and are responsible for few, if any, obvious behavioral effects.[3−6] The arachidonic acid-derived endocannabinoid lipids anandamide (AEA)[7] and 2- arachidonoylglycerol (2-AG)[8] nonselectively activate both CB receptors. Since endocannabinoids (eCBs) are rapidly degraded, metabolically stable agonists that selectively target CB1Rs and CB2Rs have proven useful tools to elucidate their physiological roles and to modulate the endocannabinoid system (ECS).[9,10] Importantly, the tissue protective role of CB2Rs in pathophysiological processes related to inflammation and their lack of central effects have rendered them an attractive drug target.[11] Consequently, structurally diverse CB2R-selective agonists are being developed as drug candidates[12] for various diseases/pathological conditions ranging from chronic and inflammatory pain,[13] pruritus,[14] diabetic neuropathy,[15] liver cirrhosis,[16] and various types of ischemic-reperfusion injury,[17−19] to autoimmune, kidney, and fibrotic diseases.[4−6,15,20−26] Although during the last two decades numerous selective and potent CB2R ligands belonging to diverse chemical scaffolds have been described in the scientific and patent literature, only a handful of synthetic ligands reached the clinical stage of development.[12,27] The reason for this may partly be attributed to the lack of knowledge regarding the different physiological roles of CB2Rs in cells and tissues. The use of conditional CB2R (*Cnr2*) knockout mice significantly contributed to elucidate the role of CB2Rs in diverse pathophysiological conditions including liver and kidney inflammation and fibrosis.[6,15,20,21,28,29] Yet pharmacological probes bearing optimal pharmacokinetic (PK) properties represent a nonredundant complementary aid for target validation *in vivo*. An international consortium has previously profiled available CB2R ligands for basic research and concluded that JWH-133 and HU-308, which are synthetic cannabinoids were the best profiled CB2R agonists *in vivo*.[30]

Nonetheless, due to their high lipophilicity, relatively low solubility, and strong binding to plasma proteins, synthetic cannabinoids show suboptimal PK properties. Therefore, the generation and characterization of novel CB2R agonists

Received: May 7, 2024
Revised: June 26, 2024
Accepted: July 2, 2024
Published: July 9, 2024

combining high potency with (a) high selectivity over other targets, especially the CB1R; (b) favorable physicochemical properties including a balanced mixture of lipophilicity and water solubility; and (c) good bioavailability are crucial for pharmacological *in vivo* testing. Furthermore, the use of brain-impermeable ligands is desirable for peripheral indications such as acute or chronic kidney diseases.

In the absence of comparable and comprehensive *in vitro* assessments of promising CB2R scaffolds published in the scientific and patent literature, we synthesized five highly potent CB2R agonists: A-796260[31] (**RNB-92**) and **RNB-61** from Abbott,[32] **RNB-73** from Amgen[33] and **RNB-90**[34] and **RNB-70**[35] from the Boehringer Ingelheim. These compounds were selected to achieve the highest structural diversity with the minimal number of compounds and based on the limited pharmacological data revealed within the patent, primarily CB2R binding potency. We characterized their CB2R binding affinity and CB2R selectivity over CB1R, as well as physiochemical and pharmacokinetic properties.

RNB-61, which was not previously profiled in the patent in depth,[32] exhibited the highest selectivity toward CB2Rs in our assay and thus was thoroughly interrogated on its receptor pharmacology, bioavailability, PK, and metabolism. Because numerous recent studies have demonstrated the protective effects of CB2R signaling in various relevant preclinical models of acute and chronic kidney diseases (e.g., induced by ischemia/reperfusion (I/R), chemotherapy drug cisplatin, advanced liver injury (hepatorenal syndrome), chronic diabetes, and unilateral ureteral obstruction (UUO),[15,20−26,29] we also tested the efficacy of the compound in models of acute or chronic kidney injury/inflammation and/or fibrosis induced by renal I/R in mice or UUO in rats.

MATERIALS AND METHODS

Synthesis of RNB Compounds. The synthesis of **RNB-61**, **RNB-70**, **RNB-73**, **RNB-90**, and **RNB-92** were performed as described in the literature.[31−35] The synthesis of **RNB-61** and its regioisomer was accomplished as depicted in Scheme S1 and is described in more detail in the Supporting Information. Briefly, the tosylate (**1**) was reacted with hydrazine hydrate and immediately converted in a [2 + 3] cycloaddition reaction to pyrazol (**2**). Subsequent amide coupling using 2-fluoro-5-trifluoromethylbenzoyl chloride provided amide (**3**) in 66% yield. Regioselective methylation of the pyrazol N1 position using dimethyl sulfate generated tetra-substituted pyrazol (**4**) in 52% yield. Via nucleophilic aromatic substitution with 2-methylpropane-1,2-diol in the presence of potassium *tert*-butoxide the synthesis of **RNB-61** was finalized. Importantly, reaction of the amide with dimethyl sulfate in the presence of potassium carbonate led selectively to amide nitrogen methylation yielding the regioisomer of **RNB-61**.

Synthesis Procedures for Radioligands. *[^{3}H]RNB-61*. The *N*-desmethyl precursor of **RNB-61** (1.0 mg, 2.14 μmol) was added to a solution of [^{3}H]methyl 4-nitrobenzenesulfonate (1.85 GBq, 0.160 mg, 0.714 μmol) in 50 μL of toluene (dried over aluminum oxide Woelm B Super I) in a screw-top vial and heated to 120 °C for 65 h. After evaporation of the solvent, the crude product was purified by silica gel chromatography using a mixture of dichloromethane and methanol (95:5) as eluent. The isolated fractions were analyzed by radio-TLC on silica plates (dichloromethane/methanol/triethylamine, 90:10:1). The pure fractions were pooled, the solvent was removed under reduced pressure, and the residue was dissolved in 10 mL of ethanol to yield 792 MBq (43%) of the tritium-labeled radioligand in a specific activity of 3.15 TBq mmol^{-1} (based on MS analysis) and 99.4% radiochemical purity (by radio-HPLC).

[^{14}C]RNB-61. The *N*-desmethyl precursor of **RNB-61** (209 mg, 447 μmol) was added to a solution of [^{14}C]methyl 4-nitrobenzenesulfonate (925 MBq, 97.8 mg, 446 μmol) in 1.5 mL of toluene (dried over aluminum oxide Woelm B Super I) in a screw-top vial and heated to 120 °C for 21 h. After evaporation of the solvent the crude product was purified by silica gel chromatography using a mixture of dichloromethane, methanol, and triethylamine (97:3:0.5) as eluent. The isolated fractions were analyzed by radio-TLC on silica plates (dichloromethane/methanol/triethylamine, 90:10:1). The pure fractions were pooled, and the solvent was removed under reduced pressure to yield 76.5 mg (307 MBq, 33%) of the ^{14}C- labeled target compound as white solid in a specific activity of 1.94 GBq mmol^{-1} (based on MS analysis) and 99.2% radiochemical purity (by radio-HPLC).

Receptor Binding and Activity Assays. Competition and saturation binding assays were performed using the radiolabeled CB1R/CB2R agonist [^{3}H]-CP55940 (PerkinElmer). Competition assays were conducted by incubating membrane protein fractions from human embryonic kidney (HEK) cells expressing the human CB1R or CB2R with 1.5 nM [^{3}H]-CP55940 in the presence or absence of increasing concentrations of **RNB-61** for 2 h at 30 °C in a final volume of 0.2 mL of assay buffer (50 mmol L^{-1} Tris-HCl, 5 mmol L^{-1} MgCl2, 2.5 mmol L^{-1} EDTA, and 0.5% fatty acid-free BSA [pH 7.4] and 1% DMSO), with gentle shaking. Saturation binding assays were conducted by incubating membrane protein fractions from HEK cells with 12 concentrations in the range of 80−0.039 nM [^{3}H]-CP55940 for 2 h at 30 °C in a final volume of 0.2 mL per well of assay buffer without DMSO. WIN55212−2 (PerkinElmer) (10 μM) was used to define nonspecific binding; > 95% of the total binding signal was specific.

Binding reactions were terminated by vacuum filtration onto 0.5% polyethylenimine presoaked GF/B filter plates (Packard) using a Filtermate cell harvester followed by 6 brief washes with 0.3 mL/well of ice-cold wash buffer. Wash buffer comprising 50 mmol L^{-1} Tris- HCl, 5 mmol L^{-1} $MgCl_2$, 2.5 mmol L^{-1} EDTA, and 0.5% fatty acid-free BSA, pH 7.4. Plates were dried at 50 °C for 1 h and liquid scintillation counting was used to determine levels of bound radiolabel. IC_{50} values and Hill slopes were determined with a 4-parameter logistic model using ActivityBase (ID Business Solution, Guilford, UK) and pKi values were determined using the Cheng−Prusoff equation as shown below:

$$pKi = \frac{\text{IC50}}{\left(1 + \frac{S}{\text{Km}}\right)}$$

where *S* indicates the concentration of the substrate and Km depicts the affinity constant of the substrate. Binding data for 80 additional receptors was carried out at Eurofins Scientific (CEREP) and is reported as the average **RNB-61** induced percent inhibition of the binding of reference compounds in two measurements.

Functional CB2R activity was assessed with the cyclic AMP (cAMP) assay (DiscoveRx, Fremont, CA, USA) using the cAMP-Nano-TRF detection kit (Roche Diagnostics, Penzberg,

https://doi.org/10.1021/acsptsci.4c00269
ACS Pharmacol. Transl. Sci. 2024, 7, 2424−2438

Germany) in Chinese hamster ovary (CHO) cells recombinantly expressing human wild type, human Q63R variant, cynomolgus, canine, rat, and mouse CB2R as reported previously.[30] We further characterized CB2R activity in CHO cells expressing human wild-type CB2R with the established [^{35}S]GTPγS assay and β-arrestin2 assay (Pathhunter assay, DiscoverX) as described previously.[30] Binding and functional assessment of the other endocannabinoid targets (FAAH, MAGL, ABHD6, ABHD12, EMT, COX-2, TRPV1, TRPA1, GPR55, PPARg) was done as depicted in our previous report.[36]

Tissue Radioligand Experiments Using [^{3}H]RNB-61 and [^{14}C]RNB-61. For the radioligand experiments, 10-week-old male C57BL/6J mice and the CB2R knock-out mice on a C57BL/6J background (B6.129P2-*Cnr2*^{tm1Dgen}/J) were obtained from the Jackson Laboratory (Bar Harbor, ME). The donating investigator reported the *Cnr2*$^-$ mice were backcrossed at least five generations to C57BL/6J mice prior to sending to The Jackson Laboratory Repository. The CB2R knockout allele was created by Deltagen by electroporating the "Neo555T" construct into 129P2/OlaHsd- derived E14 embryonic stem (ES) cells resulting in a 334 bp deletion in the coding exon of CB2R locus on chromosome 4. C57BL/6J mice or CB2R knock-out mice were used in a model of LPS challenge. The lipopolysaccharide (LPS) challenge was carried out by injecting 1 μg of LPS per mouse i.p. 30 min after application of test compounds. Six hours later, mice were killed by cervical dislocation under deep anesthesia using xylazine (10 mg kg^{-1})/ketamine (100 mg kg^{-1}). Spleens were removed and either used for membrane preparation or sliced on a cryostat at −20 °C. Slices were 20 μm thick, transferred to gelatin-coated slides, and kept dry at −80 °C. For histological control, adjacent sections were stained with hematoxylin/eosin. Frozen spleen samples were homogenized in 210 mM sucrose, 40 mM NaCl, 2 mM ethylene glycol-bis (β-aminoethyl ether) *N*,*N*,*N*′,*N*′-tetraacetic acid, 30 mM HEPES (pH 7.4), and 0.35 mg mL^{-1} PMSF at pH 7.4, using a polytron homogenizer (Kinematica, Switzerland). Total spleen membranes were then recovered by centrifugation at 100 000*g* at 40 °C for 90 min. The pellets were resuspended in 10 μL mg^{-1} of 10 mM Tris−HCl and 1 mM EDTA (pH = 7.4), and then 4 μL mg^{-1} of 20% SDS was added. Samples were then centrifuged at 1100*g* for 25 min. Protein concentrations of the supernatant were determined spectrophotometrically.

Compound Stability. The stability of the compound was assessed using the aqueous stability assay (ASTA), as previously described.[37] In short, aqueous solutions of **RNB-61** were prepared at 5 different pH values (range 1−10), added to incubation plates and shaken for 10 min at 37 °C. Solutions were transferred to a filter plate (Millipore MSGVN2250, pore size 0.22 μm) and filtered into V- bottom plates (ABGene, AB-0800) prior to heat-sealing. The procedure was repeated, increasing the 37 °C incubation time by 2 h. Samples were analyzed by HPLC at 0 and 2 h. A compound was classified as unstable if <90% of the initial concentration was detected after 2 h.

Solubility and Lipophilicity. For the determination of the octanol/water distribution coefficient (log*D*), the carrier-mediated distribution system (CAMDIS)-assay was used as described elsewhere.[38] Kinetic and thermodynamic solubilities were assessed using the lyophilization solubility assay (LYSA) and thermodynamic solubility assay (THESA), respectively. For the LYSA, the solubility of **RNB- 61** in phosphate buffer at pH 6.5 from an evaporated 10 mM DMSO compound stock solution was measured. Two aliquots of the test compounds were dried and dissolved in phosphate buffer at pH 6.5. The solutions were then filtered and diluted (3 different dilution levels for each compound) before high throughput mass spectrometry (MS) analysis was performed in an Agilent RapidFire system. Each test compound was quantified using a 6-point calibration curve prepared with the same DMSO starting solution. For THESA, **RNB-61** (8.6 mg per mL solvent/vehicle) was stirred in HPLC vials (9 × 12 × 32 mm, Waters) at 350 rpm for 15 h. The presence of solid particles was determined by microscopic analysis of 10 μL samples. If the active pharmacological ingredient (API) was completely dissolved, more solid API was added before stirring for another 15 h. This step was repeated for up to 96 h or until residual solid particles could be detected. Samples (0.5 mL) were transferred to Eppendorf Ultrafree filter tubes (Filter: PVDF 0.22 μm) and centrifuged at 14,500 rpm for 10 min. The filtrates were diluted in ethanol and analyzed by ultra-performance liquid chromatography (UPLC). Measurements were repeated in 0.05 M aqueous phosphate buffer and in fasted (FaSSIF) and fed (FeSSIF) simulated gastrointestinal fluids.

Hepatocyte and Microsomal Stability. The hepatocyte clearance assay was performed as previously described.[39] For mice hepatocytes, the suspension cultures were either freshly prepared by liver perfusion or prepared from cryopreserved hepatocyte batches (pooled C57BL6 mouse hepatocytes were purchased from BioreclamationIVT (NY, USA)). For human hepatocytes, commercially available, pooled (5−20 donors), cryopreserved samples from nontransplantable liver tissues were used. For the suspension cultures, Nunc U96 PP-0.5 mL (Nunc Natural, 267245) plates were used, which were incubated in a Thermo Forma incubator from Fischer Scientific (Wohlen, Switzerland) equipped with shakers from Variomag Teleshake (Sterico, Wangen, Switzerland) for maintaining cell dispersion. The cell culture medium was William's media supplemented with glutamine, antibiotics (100 IU/mL Penicillin-Streptomycin, Gibco), insulin, dexamethasone, and 10% fetal calf serum (FCS). Incubations of a test compound at 1 μM test concentration in suspension cultures of 1 × 10^6 cells mL^{-1} (~1 μg μL^{-1} protein concentration) were performed in 96-well plates and shaken at 900 rpm for up to 2 h in a 5% CO_2 atmosphere at 37 °C. After 3, 6, 10, 20, 40, 60, and 120 min, a 100 μL cell suspension in each well was quenched with 200 μL methanol containing an internal standard. Samples were then cooled and centrifuged before analysis by LC-MS/MS. Log peak area ratios (test compound peak area/internal standard peak area) or concentrations were plotted against incubation time with a linear fit. The slope of the fit was used to calculate the intrinsic clearance (CL_{int}). Microsomal clearance data were generated as previously reported by our group.[40]

Drug Metabolism, CYP and hERG Inhibition, and GSH Adduct Formation. Cytochrome P450 (CYP) assays were conducted as previously described.[41] In brief, **RNB-61** was incubated at a range of concentrations with the following components: pooled human liver microsomes, CYP probe substrate around the reported Km, and NADPH with a final concentration: 1 mM in 100 mM sodium phosphate buffer (pH 7.4). The conditions were optimized for a linear metabolic rate for the probe substrate reactions. The analysis

https://doi.org/10.1021/acsptsci.4c00269
ACS Pharmacol. Transl. Sci. 2024, 7, 2424−2438

of the samples was carried out by LC-MS/MS. The assays generated two endpoints: IC50 (μM) and percent inhibition at the highest acceptable test concentration (typically 50 μM; lower if the highest concentration data are rejected due to insolubility). Glutathione-stimulating hormone (GSH) adduct formation data was assessed as reported in a previous study.[42] Briefly, **RNB-61** was incubated with human liver microsomes to form reactive metabolites, and glutathione was added as a nucleophile to convert the reactive metabolites into stable conjugates that could be analyzed by MS. The formation of reactive metabolites suggests a test compound might trigger drug-induced liver injury and drug-induced hypersensitivity reactions in patients. *h*ERG inhibition was measured as described in a recent publication.[43]

Permeability Assays. The general permeability of the compound was assessed using the parallel artificial membrane permeability (PAMPA) assay and the permeability-glycoprotein (P-gp) assay was used to specifically test for brain penetration. PAMPA data were generated as previously reported by our group.[44] The P-gp assay, which evaluates the brain penetration of test compounds, was performed as described elsewhere.[45] Briefly, transfected porcine kidney epithelial (LLC-PK1) cells expressing human or mouse P-gp were cultured on 96-well semipermeable filter membrane plates (Millipore, Darmstadt, Germany). Cells formed a polarized monolayer with tight junctions that acted as a barrier between apical and basolateral compartments. P-gp was expressed in the apical-facing membrane of the monolayer (tightness confirmed using Lucifer yellow). To determine the unidirectional permeability (Papp) of **RNB-61**, samples were added separately to the apical (for A > B Papp) and basolateral (for B > A Papp) sides of the cell monolayer (i.e., donor compartments), and **RNB-61** movement into the respective receiver compartments was measured by LC-MS/MS over a 3 h incubation at 37 °C. The effect of P-gp was measured by expressing the efflux ratio of the unidirectional A > B and B > A Papp values. The mean permeability (A > B and B > A Papp) was determined in the absence of P-gp via the addition of the selective P-gp inhibitor, tariquidar.

Animal Husbandry. All animal experiments were performed in conformity with local animal welfare regulations for the care and use of laboratory animals. The pharmacokinetics experiments were executed to conform to the Swiss Lab animal legislation under permission number 244. The I/R injury model was executed to conform to the Swiss Lab animal legislation under license number 2367/20035. The rat UUO model was executed to conform to the Swiss Lab animal legislation under license number 2463/25177. All rodents were group-housed in an AAALAC-accredited animal husbandry in Tecniplast cages (Tecniplast, Italy). Room conditions were the following: the temperature was in the range of 20−24 °C, the humidity was between 50 and 60%, and the light-dark cycle was set to 12/12 h. The maximum caging density was five mice or rats with the same litter and sex. Environmental enrichment was offered all the time (nestlets, tissue, tubes). All animals are held on a standard diet with ad libitum access to food and water.

Pharmacokinetics after Intravenous and Oral Administration. To characterize the pharmacokinetic behavior of RNB-61, studies in rodents were conducted at the *in vivo* facility of F. Hoffmann-La Roche Ltd. (Basel, Switzerland). The plasma-concentration time profile was studied in rodents after single-dose **RNB-61** administration by oral gavage (p.o. microsuspension excipients 7.5% gelatin/0.62% NaCl) and intravenous bolus injection (i.v. solution, excipients NMP:NaCl (30:70)). Three groups of male Wistar rats (n = 2 per group) were administered **RNB-61** either at 1 mg kg^{-1} i.v., 3 mg kg^{-1} p.o., or 26 mg kg^{-1} p.o. Plasma samples were drawn at 0.083, 0.25, 0.5, 1, 2, 4, 8, and 24 postdose in the i.v. group and at 0.25, 0.5, 0.75, 1.5, 3, 5, 8, and 24 h postdose in the p.o. groups. The samples were analyzed for **RNB-61** concentration by LC/MS-MS. For the LC/MS-MS analysis, and the samples were prepared by adding 100 uL to 400 uL ACN with ISTD (100 ng/mL Bosantan in ACN/MeOH 1/1), stirring, and centrifuging (4000 rpm, 65'). 100 uL of the supernatant were pipetted and diluted with 400 μL H_2O at pH 3. The analytes were separated on a Restek C18 column (5 μm, 1.0 × 3 mm). The mobile phase consisted of water containing 0.1% HCOOH as solvent A and ACN containing 0.1% HCOOH as solvent B. The gradient curve starting with 5% B was changed to 90% B between 0.4 and 0.6 min and further increased to 95% B between 0.6 and 1.2 min. This was maintained until 1.4 min and then reduced and kept at 5% B between 1.45 and 2.0 min. The mass spectrometer was operated in the positive mode. All LC-MS/MS was done using the Agilent RapidFire Analyzer software (version 4.3). The pharmacokinetic parameters were estimated by noncompartmental analysis in the Certara WinNonlin software (version 5.3). A similar study design was run in mice with three groups receiving 2 mg kg^{-1} i.v., 4 mg kg^{-1} p.o., or 26 mg kg^{-1} p.o., and plasma sampling occurring in a composite profile (n = 2 for each time point) up to 7 or 24 h postdose. Male C57/BL6 mice (n = 5 per group) were used to study the influence of P-gp efflux on brain penetration. Two groups of mice were administered **RNB-61** by i.v. bolus injection at 1 mg kg^{-1} (2 groups). In order to block P-gp activity, an i.v. bolus of 5 mg kg^{-1} tariquidar[46] was injected into one group 30 min prior to **RNB-61**. Plasma was collected at 0.083, 0.25, 0.5, 2, 4, and 7 h postdose in a composite profile. Brain, CSF, and vitreous body were collected at terminal time points 0.5, 2, 4, and 7 h postdose.

Kidney Disease Models. In the ischemia/reperfusion (I/R) model of acute kidney injury (AKI),[47,48] the compounds were administered orally by gavage to C57BL/6 mice 30 min before ischemia obtained by clamping both renal arteries and veins for 25 min, followed by 24 h of reperfusion. Mice were anesthetized using xylazine (10 mg kg^{-1})/ketamine (100 mg kg^{-1}) injected intraperitoneally. Sham treated mice were treated identically except for the temporary closure of the renal vessels. After 24 h, under reanesthesia, plasma was taken for biomarker analysis. Thereafter, mice still in deep anesthesia were sacrificed by cervical dislocation. Creatinine, BUN (blood urea nitrogen), NGAL (neutrophil gelatinase-associated lipocalin), osteopontin, and KIM1 (kidney injury molecule-1) levels were determined using the following commercially available standard assays: creatinine: Roche Diagnostics 03263991, BUN: Roche Diagnostics 04460715, NGAL: BioPorto, Kit046 + Kit042, osteopontin: R&D Systems, MOST00, KIM-1: Abnova, KA1064. To assess fibrotic effects, we used the unilateral ureteral obstruction (UOO) model in Sprague−Dawley rats.[49] For the UOO model, rats were sacrificed after 5, 8, and 11 days and the percentage of PicroSirius Red positive areas (indicator of collagen III−I deposition) were measured in 4 μm histological cross sections of the kidney after 2% paraformaldehyde perfusion fixation and paraffin embedding. The extend of kidney fibrosis was

https://doi.org/10.1021/acsptsci.4c00269
ACS Pharmacol. Transl. Sci. 2024, 7, 2424−2438

quantified based on PicroSirius Red staining of 10 renal sections about 1 mm apart from each kidney. The collagen−III-I-positive pixel counts were determined in the cortical aspect of each kidney section from 10 optical fields using a 40× objective. As the total area analyzed was identical for all kidneys under investigation, the absolute number of pixels was used as the relevant readout. Vehicle treated animals received saline gavage only. The details of PicroSirius Red staining were previously described.[22]

Data Analysis and Statistics. All statistical analysis was carried out in Python 3.9 using the SciPy package (version 1.13.1). The visualization of data was carried out using the Seaborn package (version 0.13.2) in a Python 3.9 environment. For the binding and functional assays, a 4-parameter logistic model was used (ActivityBase, IDBS, version 9.4). For pharmacokinetics (noncompartmental analysis), we used the Certara Phoenix WinNonlin software (version 5.3). Data are represented as mean ± standard deviation unless otherwise indicated. Statistical significance was determined using the Mann−Whitney test with the Bonferroni correction where applicable unless otherwise stated ($^{ns}p > 0.05$, $^{*}p < 0.05$, $^{**}p < 0.01$, $^{***}p < 0.001$, $^{****}p < 0.0001$).

RESULTS

RBN-61 Is a Highly Potent and Selective CB2 Receptor-Specific Ligand. With the aim to identify an optimal CB2R tool compound, we synthesized five highly potent CB2R agonist found in the patent literature: A-796260[31] (**RNB-92**) and **RNB-61** from Abbott,[32] **RNB-73** from Amgen,[33] and **RNB-90**[34] and **RBN-70**[35] from the Boehringer Ingelheim (Figure 1). The binding interactions of these CB2R agonists with cannabinoid receptors were assessed on both CB1Rs and CB2Rs, respectively (Table 1). Out of the five ligands, **RBN-61** potently bound to human CB2R (*h*CB2R) with an apparent K_i value of 0.57 ± 0.03 nM and exhibited the best-in-class 6,800-fold selectivity over *h*CB1R (K_i value = 4.3 μM) (Table 1). The regioisomer of **RNB-61** with the methylated amide (Figure 1) was inactive (data not shown). In line with the binding affinity on *h*CB2Rs, the K_i value of **RNB-61** for mouse CB2R (*m*CB2R) was 1.33 ± 0.47 nM, with an *m*CB2R/*h*CB2R K_i ratio of 2.3, which was slightly higher than for **RNB-73** (0.56). The range of K_i values for the selected ligands were in line with the EC_{50} values obtained in the cAMP inhibition assays (Table 1). **RNB-61** also had favorable solubility, lipophilicity, clearance, and permeability in comparison to the four other molecules (Table 1). In addition to CB1R, **RNB- 61** also exhibited a great selectivity over the other endocannabinoid system (ECS) targets, lacking interactions and functional effects up to 10 μM for FAAH, MAGL, ABHD6, ABHD12, endocannabinoid membrane transporter (EMT), and COX-2 (Table S1). The specificity of the compound against other ECS targets was evaluated functionally. **RNB-61** did not inhibit the hydrolysis (FAAH, MAGL and ABHDs), oxygenation (COX-2), and cellular AEA uptake (EMT) of ECs at the screening concentration of 10 μM (Table S1). Next, a thorough characterization of **RBN-61** receptor pharmacology against 80 additional receptors, including dopamine, serotonin, epinephrine, norepinephrine, acetylcholine, GABA, benzodiazepine, opioid, adenosine, prostaglandin, and chemokine receptors, among others, was conducted using CEREP (now Eurofins). **RNB-61** showed no significant binding (defined as ≥50% of probe displacement) to most receptors at the screening concentration of 10 μM (Figure S1). The one exception was the Na^+ ion channel site 2, for which 10 μM of **RNB-61** inhibited 96% of [^{3}H]-batrachotoxin binding. Follow-up measurements with 1 μM and 0.1 μM of **RNB-61** showed 32% and no inhibition of [^{3}H]-batrachotoxin binding, respectively, indicating no potential off-target interactions at physiologically relevant concentrations (<1 μM), thus supporting the very high selectivity of **RBN-61** toward CB2R (Figure S1).

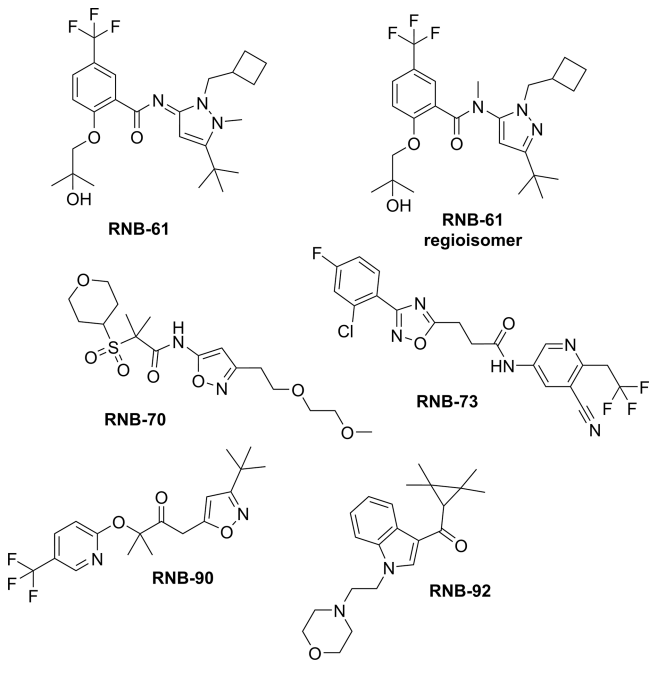

Figure 1. Chemical structures of RNB compounds.

RBN-61 Is a CB2 Receptor Full Agonist. A further characterization of the functional activity of **RBN-61** on *h*CB2R was performed measuring G-protein activation ([^{35}S]GTPγS binding assay), cAMP formation and β-arrestin2 recruitment. As expected, **RBN-61** induced a concentration-dependent increase in G-protein activation (EC_{50} = 0.33 ± 0.09 nM) and β-arrestin2 recruitment (EC_{50} = 13.3 ± 1.9 nM), while it inhibited forskolin (FSK)-driven cAMP formation (EC_{50} = 1.65 ± 0.96 nM) (Figure 2). The functional modulation of CB2R activity occurred at a similar concentration range as the K_i and K_d value calculated for the binding. **RBN-61** induced the same efficacy (E_{max}) as CP55,940 for the inhibition of cAMP formation and G-protein activation, while reaching approximately 80% E_{max} of total β-arrestin2 recruitment (Figure 2). To decipher whether RNB-61 is suitable for the elucidation of the pharmacology of CB2R in different animal disease models, we next performed the cAMP assay with CB2R from species of preclinical interest as well as the common human missense variant CAA/CGG (Q63R). As shown in Table 2, **RNB-61** inhibited the FSK-induced cAMP formation on mouse, rat, dog, and monkey CB2Rs with EC_{50} values ranging from 0.13 to 1.86 nM, which were in line with the EC_{50} value toward the wild-type *h*CB2R (0.31 ± 0.07 nM). Similarly, the EC_{50} value for the Q63R human variant was 0.29 ± 0.05 nM.

[^{3}H]-RNB-61 and [^{14}C]-RNB-61 as Radiopharmaceutical Tools. Next, we validated radiolabeled versions of **RNB-61** by labeling CB2R expressing membrane preparations from cells and intact tissues. In labeling membrane preparation of

https://doi.org/10.1021/acsptsci.4c00269
ACS Pharmacol. Transl. Sci. 2024, 7, 2424−2438

Table 1. Comparison of the Selectivity toward Human CB2 (*h*CB2) Receptors of Five Representative Molecular Scaffolds

	RNB-92	RNB-73	RNB-90	RNB-70	RNB-61
K_i *h*CB2R (nM) (binding assay)	0.85 ± 0.44 (n = 3)	65.3 ± 15.8 (n = 3)	0.39 ± 0.21 (n = 3)	17.92 ± 9.2 (n = 3)	0.57 ± 0.03 (n = 3)
K_i *h*CB1R (nM) (binding assay)	-	>10,000 (n = 1)	120 ± 2.48 (n = 3)	>10,000 (n = 3)	3882 ± 73.4 (n = 3)
*h*CB2R selectivity	-	>153	307	>559	6810
K_i *m*CB2R (nM) (binding assay)	6.53 ± 1.18 (n = 3)	36.9 ± 17.8 (n = 3)	1.53 ± 0.38 (n = 3)	266 ± 68.9 (n = 3)	1.33 ± 0.47 (n = 3)
*m*CB2R/*h*CB2R	7.68	0.56	3.9	14.8	2.3
EC_{50} *h*CB2R (cAMP assay)	0.17 ± 0.01 (n = 2)	7.13 ± 2.19 (n = 2)	0.26 ± 0.05 (n = 2)	13.04 ± 2.58 (n = 2)	0.31 ± 0.07 (n = 8)
EC_{50} *h*CB1R (cAMP assay)	933 ± 136 (n = 3)	>10,000 (n = 3)	19.6 ± 1.18 (n = 3)	>10,000 (n = 3)	>10,000 (n = 1)
solubility (μg/mL)	2	<1	<1	>510	250
log*D*	3.43	3.86	4.07	0.8	3.34
$PAMPAP_{eff}$ (cm/s × 10^{-6})		7.4	2	5.9	2.14
microsomal CL_{int} human (μL/min/mg protein)	420	<10	15	<10	≤10
microsomal CL_{int} rat (μL/min/mg protein)	730	<10	81		<10

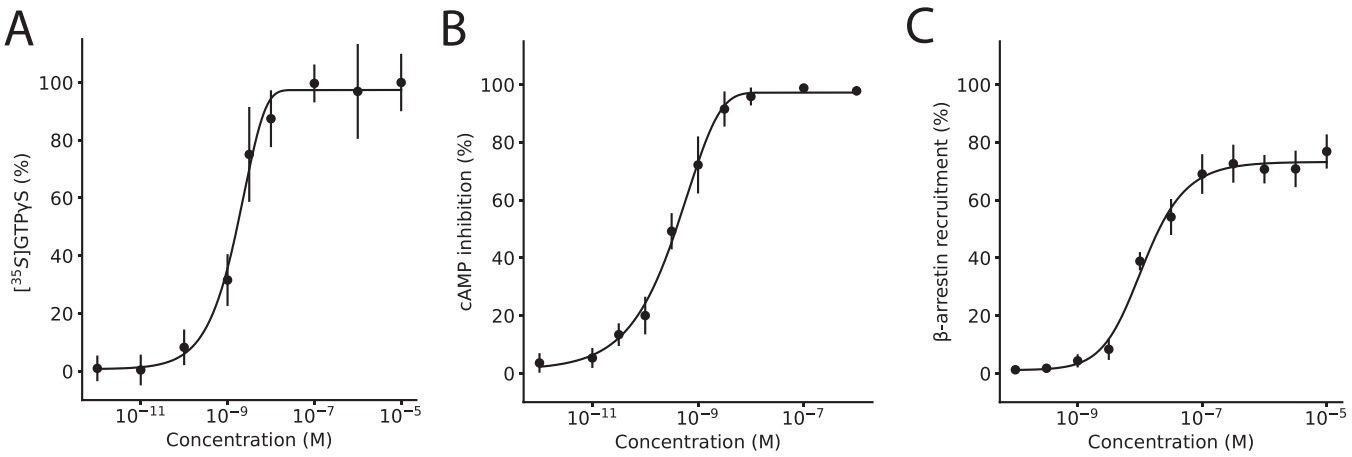

Figure 2. Concentration−response of RNB-61 on [^{35}S]GTPγS binding, cAMP inhibition, and β-arrestin recruitment. (A) Concentration−response of **RNB-61** on G-protein coupled receptor activation expressed as the percentage of binding of the nonhydrolyzable GTP analog [^{35}S]GTPγS (n = 4, in triplicates, EC_{50} = 1.65 ± 0.96 nM, E_{max} = 100). (B) Concentration−response of **RNB-61** on cyclic AMP (cAMP) inhibition expressed as the percentage, normalized to 1 μM of CP55940 (n = 6, in triplicates, EC_{50} = 0.33 ± 0.09 nM, E_{max} = 100). (C) Concentration−response of **RNB-61** on β-arrestin2 recruitment expressed as a percentage, normalized to 1 μM of CP55940 (n = 6, in triplicates, EC50 = 13.3 ± 1.9 nM, Emax = 80).

Table 2. Comparison of EC_{50} values on cAMP production expressing CB2 from different species and the human Q63R mutant

	cAMP assay − CB2R
	EC_{50} values (mean ± SD, nM)
human wild type	0.31 ± 0.07 (n = 8)
human Q63R	0.29 ± 0.07 (n = 3)
mouse	0.25 ± 0.13 (n = 4)
rat	0.13 ± 0.07 (n = 2)
dog	1.86 ± 1.58 (n = 2)
monkey	0.70 ± 0.03 (n = 2)

CHO cells overexpressing the *h*CB2 receptors, [^{3}H]-RNB-61 exhibited a K_d value of 3.08 ± 0.61 nM and [^{14}C]-RNB-61 showed a K_d value of 3.62 ± 2.31 nM, thus both being in the range of the binding interaction data (Figure 3). No nonspecific labeling was observed below 50 nM for [^{3}H]-**RNB- 61** with a corresponding signal-to-background value of 6.0 at 250 nM, whereas for [^{14}C]-**RNB- 61**, the signal-to-background value was 1.6 at 250 nM. Next, we labeled *ex vivo* spleen slices from mice with 200 nM of [^{14}C]-**RNB-61**, which showed a prominent increase in radioactivity that could be competed with 10 μM of the nonselective CBR agonist, WIN 55,212−2 and was not detected in a CB2R KO mouse strain (Figure 3). We further elucidated the CB2R specificity of [^{3}H]-**RNB-61** on spleen membranes in both rats and mice. In wild-type rat and mice spleen membranes, the radioactivity could compete away with both 10 μM WIN 55,212−2 and 1 μM of the CB2R specific antagonist SR144528 (SR2); however, no significant reduction in the radioactivity was observed with 1 μM the CB1R specific antagonist SR141716A (SR1 or rimonabant) (Figure 3). Next, we evaluated the utility of **RNB-61** for CB2R expression in 17 different cell lines that included Chinese hamster ovary (CHO) cells that recombinantly express *h*CB1R or *h*CB2R, immune cells (HL-60, U937, Jurkat, RAW264.7, HMC-1, BV2), neuronal cells (SH-SY5Y, Neuro2a, NT18G2), and miscellaneous cell lines (HeLa, PC-12, HEK-293, HPKV). Out of the 17 cell lines, the *h*CB2R-overexpressing CHO cells, and all immune cells except for HMC-1 (P value = 0.31) showed a statistically significant difference in radioactivity between the vehicle and the WIN55,212−2 preincubated samples (Figure 3). To confirm the differential CB2R radiolabeling induced in inflammatory conditions, we measured CB2R expression using [^{14}C]-**RNB-61** in *ex vivo* spleen slices from mice challenged with lipopolysaccharide (LPS). We detected a significant increase in radioactivity after 6−24 h of the introduction of LPS in the spleen, which was completely absent in the CB2R KO mouse strain (Figure 3).

https://doi.org/10.1021/acsptsci.4c00269
ACS Pharmacol. Transl. Sci. 2024, 7, 2424−2438

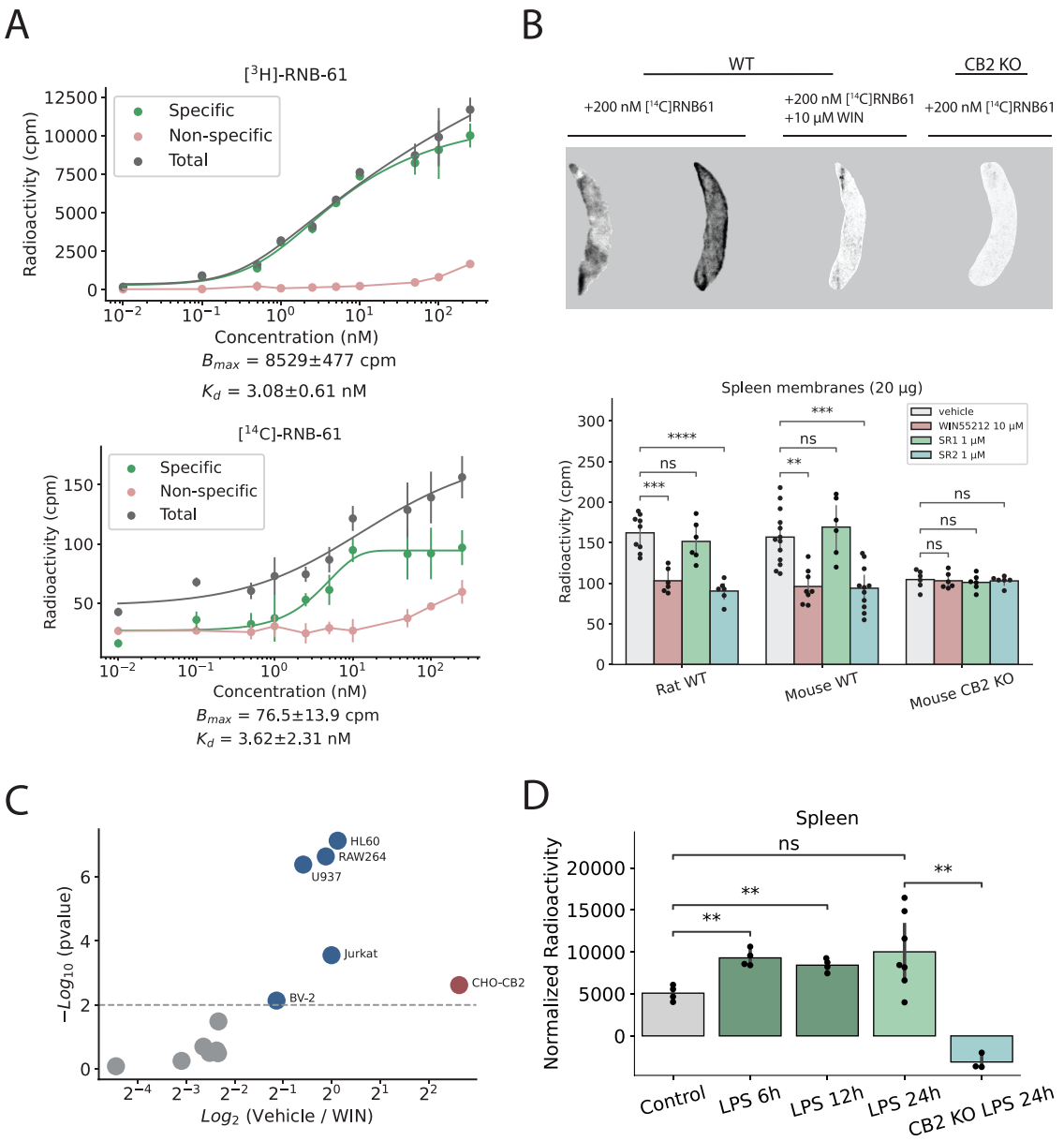

Figure 3. [^{3}H]-RNB-61 and [^{14}C]-RNB-61 to label CB2 receptors. (A) Concentration−response of membrane binding of [^{3}H]-**RNB-61** and [^{14}C]-**RNB-61** on CHO cells recombinantly expressing the human CB2R (*h*CB2R) (n = 4−6, B_{max} = 8529 ± 477 cpm, K_d = 3.08 ± 0.61 nM for [^{3}H]-**RNB-61** and B_{max} = 76.5 ± 13.9 cpm, K_d = 3.62 ± 2.31 nM for [^{14}C]-**RNB-61**). The nonspecific binding was calculated by preincubating the cells with 10 μM of WIN 55,212−2. (B) The top image depicts four representative images of spleen slices incubated in 200 nM of [^{14}C] **RNB-61**. Images were acquired using the Typhoon FLA 9500 imaging system. The bottom plot depicts the radioactivity of spleen membrane preparations from either wild-type (WT) rat, WT mouse, or the CB2R knockout mouse strain (n = 6−13 spleen slices of 3 animals for each condition). In the WT rat and mouse, the addition of 10 μM of the nonspecific CBR agonist WIN55,212−2 resulted in a significant reduction in the detected radioactivity in cpm ($p < 0.01$, $p < 0.001$ for WT rat and WT mouse, respectively, independent t test). The addition of 1 μM of the CB1R selective SR1 did not result in a significant difference, whereas the addition of 1 μM of the CB2R selective SR2 significantly reduced radioactivity ($p < 0.001$, $p < 0.0001$ for WT rat and WT mouse, respectively, independent t test). No difference in radioactivity was observed for the CB2R KO mice in any condition. (C) 17 different cell lines (CHO cells, immune cells, neuronal cells, miscellaneous cells) were incubated with 1 nM of [^{3}H]-**RNB-61** and either vehicle or 1 μM of WIN55,212−2. The volcano plot depicts the difference between the vehicle and the WIN-treated cells on the x axis and the negative logarithm of the p-value on the y-axis. Only the *h*CB2 overexpressing CHO cells and immune cells were statistically significant in CB2R-specific labeling ($p < 0.01$). No significant labeling was detected in any of the neuronal cell lines (SHSY5Y, Neuro2a, NT18G2). (D) CB2R expression measured in cpm in *ex vivo* spleen slices from mice challenged with LPS detected with the administration of 200 nM [^{14}C]**RNB-61**. The bar chart depicts the specific signal, which was attained by subtracting the nonspecific signal (10 μM of WIN-55,212 co- incubation). LPS induced a statistically significant increase in CB2R expression at various time points (6−24h), which was completely absent in the CB2R KO mice.

Physicochemical Profile and Stability. The physicochemical profile and stability of **RNB-61** were further evaluated in detail (Table 3). **RNB-61** showed a low partition coefficient (logD = 3.3), indicating moderate lipophilicity, which accounts for a good balance between solubility and permeability. Accordingly, **RNB-61** was stable in aqueous solution for 2 h at 37 °C at different pH values (1, 4, 6.5, 8 and 10) and showed a high solubility in four different assays (LYSA

https://doi.org/10.1021/acsptsci.4c00269
ACS Pharmacol. Transl. Sci. 2024, 7, 2424−2438

Table 3. Physicochemical and ADMET Properties of RNB-61

molecular weight	481.556
pK_a	7.33
clogP	3.34 (logD)
polar surface area	51 Å^2
hydrogen bond donors	1
stability in aqueous solution at pH 1, 4, 6.5, 8, 10	104.4, 102.7, 102.7, 100.5, 101.6% of initial [200 nM]
aqueous solution LYSA, THESA, FaSSIF, FeSSIF	194, 316, 630, 1373 μg mL^{-1}
melting point	188 °C
PAMPA P_{eff} (%Acc/%Mem/%Don)	2.14 × 10^{-6} cm s^{-1} (6/72/22)
P-gp transporter ER human	40.6
P-gp transporter ER mouse	26.8
Microsomal CL_{int} human, rat, mouse	≤10 μL min^{-1} (mg protein)$^{-1}$
hepatocyte CL_{int} human, mouse	85, 48.5 μL min^{-1} (10^6 cells)$^{-1}$
IC_{50} CYP450 3A4, 2C9, 2D6 inhibition	35.5, 50, 15.5 μM
GSH (human liver microsomes)	no adducts detected
*h*ERG inhibition	>10 μM
fraction unbound in plasma (human, rat, mouse)	1.9, 1.7, 1.9%

= 194 μg mL^{-1}; THESA = 316 μg mL^{-1}; FaSSIF = 630 μg mL^{-1}; FeSSIF = 1373 μg mL^{-1}). In the PAMPA assay, RNB-61 permeated through the cell membrane with an effective permeability (P_{eff}) of 2.14 × 10^{-6} cm s^{-1}, indicating a relevant permeability in cellular membranes. An estimation of the blood-brain-barrier penetration was performed *in vitro* using human and mouse *P*-glycoprotein overexpressing systems. The results showed a remarkably high P-gp efflux ratio (ER) suggesting that **RNB-61** is a strong P-gp substrate and might not reach bioactive concentration in the CNS. In further *in vitro* studies the metabolic stability of **RNB-61** was assessed, showing a low intrinsic clearance in purified microsomes and hepatocytes. Furthermore, the ligand did not affect the activity of the three most relevant cytochrome P450 isoenzymes 2C9, 2D6, 3A4 (IC_{50} value > 50 μM). Similarly, **RNB-61** did not form any adducts with glutathione in human nor in rat liver microsomes and it did not interact with the *h*ERG channel up to a concentration of 10 μM (Table 3). Overall, **RNB-61** showed a favorable balance between lipophilicity and solubility associated with optimal stability *in vitro*.

RNB-61 Pharmacokinetics and Brain Penetration. The absorption and disposition of **RNB-61** was assessed in single-dose PK studies in rodents. Upon i.v. injection of 1 mg kg^{-1} bolus in rats, **RNB-61** exhibited a low plasma clearance (CL = 3.5 mL min^{-1} kg^{-1}), in agreement with the *in vitro* CL_{int} values, and an intermediate volume of distribution (V_{ss} = 1.6 L kg^{-1}), resulting in a terminal half-life of 6.0 h (Figure 4, Table 4).

Table 4. Pharmacokinetic Parameters of RNB-61 in Rodent Models

rats	**1** mg kg^{-1}	**3** mg kg^{-1}	**26** mg kg^{-1}
route of administration	i.v.	p.o.	p.o.
C_{max} (ng mL^{-1})	619	446	1710
T_{max} (h)	0.083	5.5	3
AUC_{inf} (h ng mL^{-1})	5173	7406	117100
CL (mL min^{-1} kg^{-1})	3.5	n/a	n/a
V_{ss} (L kg^{-1})	1.6	n/a	n/a
$T_{1/2}$ (h)	6.0	7.1	49
bioavailability (%)	n/a	48	87
mice	**2** mg kg^{-1}	**4** mg kg^{-1}	**26** mg kg^{-1}
route of administration	i.v.	p.o.	p.o.
C_{max} (ng mL^{-1})	1167	843	4370
T_{max} (h)	0.25	2	2
AUC_{inf} (h ng mL^{-1})	8632	9300	47320
CL (mL min^{-1} kg^{-1})	3.9	n/a	n/a
V_{ss} (L kg^{-1})	2.4	n/a	n/a
$T_{1/2}$ (h)	7.7	6.4	4.3
bioavailability (%)	n/a	54	42

After oral administration of **RNB-61** 3 and 26 mg kg^{-1}, the compound displayed high bioavailability, suggesting nearly complete absorption in the tested dose range. The maximal plasma exposure for 3 and 26 mg kg^{-1} p.o. dosing was reached at 5.5 and 3.0 h postinjection, respectively, with C_{max} values of 446 and 1710 ng mL^{-1}. Taken together, the pharmacokinetic results indicate that in rats, RNB-61 reaches high nanomolar to micromolar concentrations in plasma after single-dose administration (C_{max}= 1285 nM, 926 nM, 3.5 μM after 1 mg kg^{-1} i.v., 3 mg kg^{-1} p.o., 26 mg kg^{-1} p.o., respectively). The overall pharmacokinetic profile was similar in mice, as depicted in Figure 4 and Table 4.

Next, we investigated the brain exposure to **RNB-61**. Upon i.v. injection of 1 mg kg^{-1}, **RNB- 61** reached the peak brain concentration of 41.3 ng mL^{-1}, which was >20-fold lower compared to the plasma level (C_{max}= 972 ng mL^{-1}) (Table 5). Similarly, the area under the curve from time zero to the last

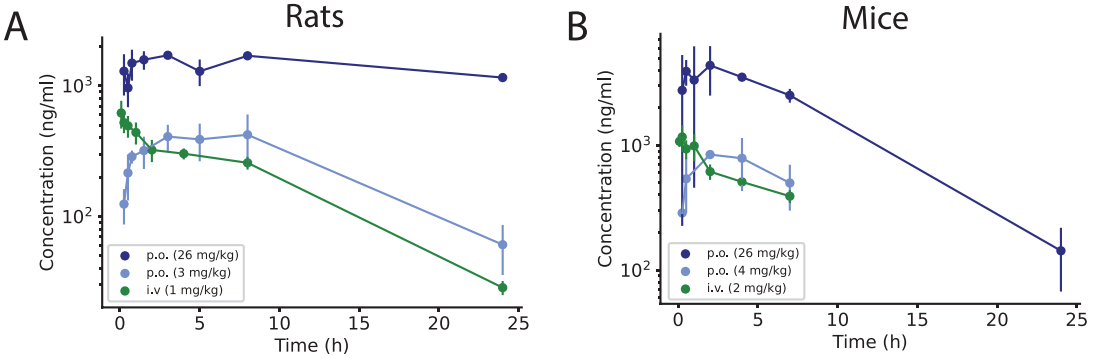

Figure 4. RNB-61 plasma pharmacokinetics after intravenous and oral administration. Plasma concentration (mean and standard deviation) of **RNB-61** after p.o. and i.v. bolus administration in (A) rats and (B) mice (n = 2 for each time point).

https://doi.org/10.1021/acsptsci.4c00269
ACS Pharmacol. Transl. Sci. 2024, 7, 2424−2438

Table 5. Brain Exposure of RNB-61 in Male C57/BL6 Mice (n = 5/group) is Enhanced By Co-Administration of Tariquidar, a P-gp Inhibitor

		plasma					
		$T_{1/2}$	T_{max}	C_{max}	AUC_{last}	AUC_{inf}	CL
RNB-61	tariquidar	h	h	ng/mL	h*ng/mL	h*ng/mL	mL/h/kg
1 mg kg^{-1}		4.00	0.25	972	2429	3318	301
1 mg kg^{-1}	5 mg kg^{-1}	3.68	0.083	737	2514	3558	281
		brain					
		$T_{1/2}$	T_{max}	C_{max}	AUC_{last}	AUC_{inf}	
RNB-61	tariquidar	h	h	ng/mL	h*ng/mL	h*ng/mL	K_p
1 mg kg^{-1}		5.98	0.58	41.3	215	375	0.088
1 mg kg^{-1}	5 mg kg^{-1}	8.42	0.53	342	1877	4386	0.747

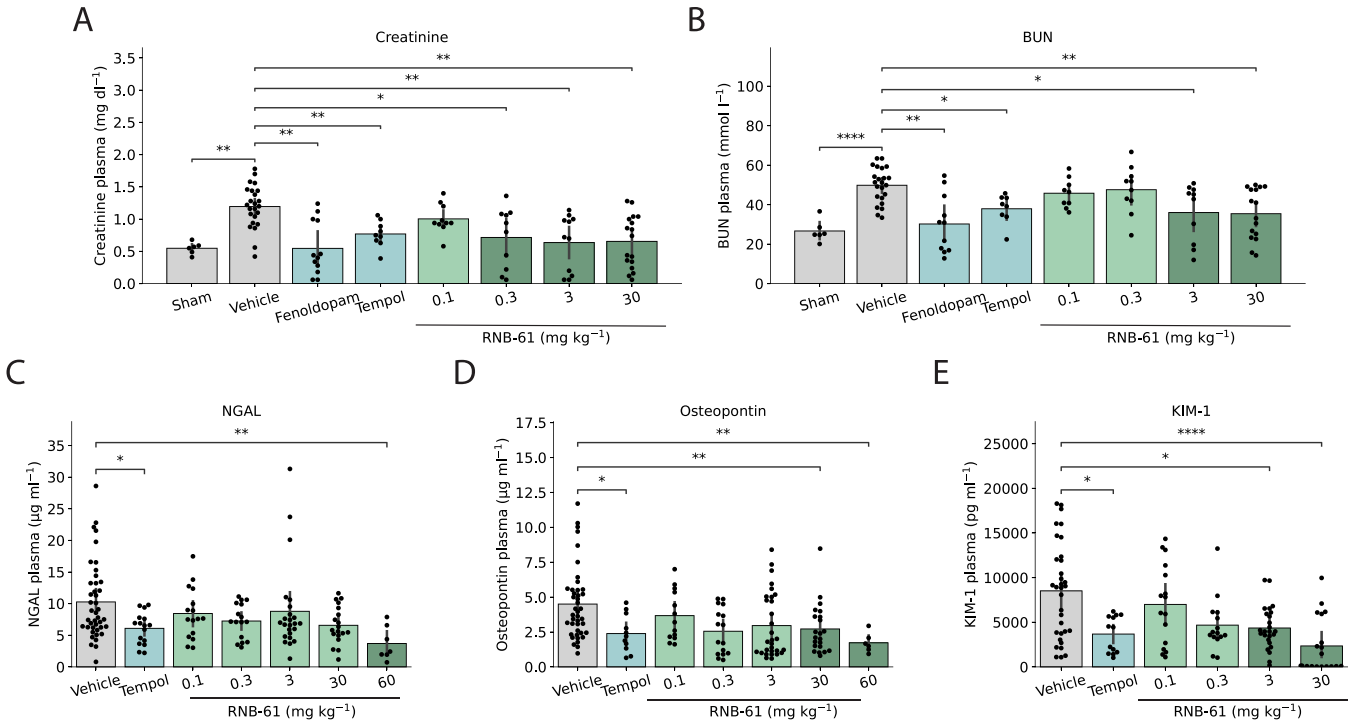

Figure 5. RNB-61 attenuates acute kidney dysfunction and injury markers induced by renal ischemia/reperfusion (I/R) in mice. (A) The administration of various concentrations of **RNB-61** alleviated I/R induced plasma creatinine levels comparable to the positive control, fenoldopam (20 mg kg^{-1}) (n = 6, 24, 12, 9, 10, 10, 12, and 17 for sham, vehicle, fenoldopam, tempol, and 0.1, 0.3, 3, and 30 mg kg^{-1} **RNB-61**, respectively). Statistical significance was determined using Mann−Whitney tests with Bonferroni correction. No significant difference was observed at 0.1 mg kg^{-1} dose for **RNB-61**. (B) For the same animals as depicted in panel (B), plasma BUN levels were measured. (C−E) For the same animals, three AKI biomarkers was also quantified (NGAL, Osteopontin, KIM-1).

measurable concentration (AUC_{last}) was >10-fold lower in the brain compared to plasma (AUC_{last}= 215 vs 2429 h × ng mL^{-1}). The brain-plasma partition coefficient (Kp, brain) of **RNB-61**, calculated as the ratio of AUC_{last} in brain and plasma, was accordingly very low (Kp= 0.088), indicating a negligible penetration into the brain. In agreement with data obtained *in vitro* showing that **RNB-61** is a P-gp substrate, upon injection of the P-gp inhibitor tariquidar (5 mg kg^{-1}), **RNB-61** reached a higher brain exposure (C_{max}= 342 ng mL^{-1}, AUC_{last}= 1877 h × ng mL^{-1}). Both parameters were ∼10-fold higher than the corresponding values after injection of **RNB-61** alone, with no apparent differences in the plasma PK profile. The significantly increased penetration into the brain was confirmed by the Kp value of 0.747 (Table 5).

RNB-61 Exerts Protective Effects in Kidney Ischemia Reperfusion (I/R) and Unilateral Ureteral Obstruction (UUO) Rodent Models. Based on its high potency and selectivity as CB2R agonist, together with the favorable PK profile, **RNB-61** represented a suitable tool compound to further investigate CB2R pharmacology *in vivo*. To validate the efficacy of **RNB-61**, evaluated its effects in two rodent models of kidney injury: the I/R-induced acute kidney injury (AKI) (Figure 5) and the UUO-induced model of chronic kidney injury (CKI), inflammation, and progressive renal fibrosis (Figure 6). In the kidney I/R model, we used the know antioxidant tempol and the clinically approved fenoldopam, an antihypertensive drug with nephroprotective effects in clinical trials of AKI, as positive controls.[50] In the I/R model, we observed an over 2-fold, significant increase (1.19 ± 0.33 mg kg^{-1}) in plasma creatinine levels compared to the sham controls (0.55 ± 0.09 mg kg^{-1}), consistent with AKI (Figure 5A, p < 0.001, independent t test). Similarly, blood urea

https://doi.org/10.1021/acsptsci.4c00269
ACS Pharmacol. Transl. Sci. 2024, 7, 2424−2438

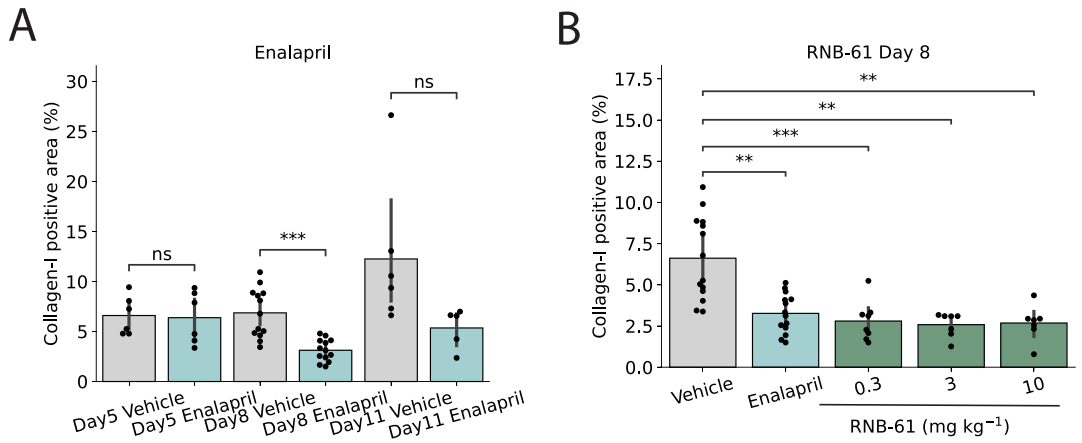

Figure 6. RNB-61 exerts nephroprotective effects in a ureteral obstruction (UOO) rat model of renal fibrosis. (A) Collagen−III-I positive area was assessed at three consecutive time points (d5, d8, and d11) for vehicle controls and rats administered with 32 mg kg^{-1} of enalapril (n = 6, 13, and 6 for d5, d8, and d11, respectively). No significant difference was observed at d5 and d11, whereas a significant reduction in the collagen-I positive area was observed at d8. (B) The collagen−III-I positive area was assessed after day 8 of the UUO in rats. A significant reduction was observed for enalapril (32 mg kg^{-1}) and for all three doses of **RNB-61** (n = 14, 14, 7, 7, and 7 for vehicle, enalapril, and 0.3, 3, and 3 mg kg^{-1} **RNB-61**, respectively, Mann−Whitney test).

nitrogen (BUN) levels increased from 26.6 ± 5.6 mg dL^{-1} in the sham control to 49.8 ± 8.9 mg dL^{-1} in the vehicle (Figure 5B, $p < 0.001$, independent t test). The I/R-induced increases in creatinine and BUN plasma levels were hampered by the pretreatment with **RNB-61** (Figure 5). The maximal protection was achieved at the dose of 3 mg kg^{-1} (48% and 30% reduction of creatinine and BUN compared to vehicle, respectively) similar to the positive control fenoldopam at 20 mg kg^{-1} (creatinine and BUN levels reduced by 55% and 39% compared to vehicle, respectively) and tempol at 50 mg kg^{-1} (creatinine and BUN levels reduced by 35% and 26% compared to vehicle, respectively) (Figure 5A-B). We used tempol as a positive control for further experiment due the lower variability compared to fenoldopam. In the same model, the AKI biomarkers neutrophil gelatinase-associated lipocalin (NGAL), kidney injury molecule-1 (KIM-1), and osteopontin were measured in plasma. In line with the effects observed on creatinine and BUN levels, **RNB-61** dose-dependently inhibited the release of all three biomarkers starting from 0.3 (NGAL and KIM-1) and 3 mg kg^{-1} (osteopontin) and reaching the maximal protection at 3−30 mg kg^{-1} (reduction by 39%, 43% and 50% compared to vehicle for NGAL, osteopontin, and KIM-1, respectively) similar to the positive control tempol (at the dose of 50 mg kg^{-1}, reduction by 43, 49, and 57% compared to vehicle for NGAL, osteopontin, and KIM-1, respectively). The nephroprotective effect of **RNB-61** was further evaluated in the UUO-induced model of kidney fibrosis in rats. Initial experiments were performed using the positive control, enalapril (32 mg kg^{-1} day^{-1}), or vehicle to identify the best time to assess the antifibrotic effect after ureteral obstruction. A significant antifibrotic effect was evident on day 8 (55% reduction vs vehicle) without any further improvement on day 11 (57% reduction vs vehicle). Thus, 8 days were chosen as a suitable duration to assess the antifibrotic effect of **RNB-61**. As shown in Figure 6, **RNB-61** exerted potent antifibrotic effects in the full range of tested doses (0.3−10 mg mL^{-1}). At 3 mg kg^{-1}, it inhibited the accumulation of collagen−III-I by 61%, which was comparable to the protective effect of the positive control enalapril (inhibition by 52%).

DISCUSSION

Although the CB2R has been validated as a drug target in numerous preclinical models, translation into effective therapeutic agents remains slow.[12,51,52] The opposite effects of CB1R and CB2R activation in numerous disease models and/or pathological conditions (e.g., liver injury/fibrosis, cardiovascular injury/fibrosis, kidney injury/fibrosis, among others) reflect the distinct roles of CB1R versus CB2R activation in various immune cells, including macrophages, Kupffer cells, osteoclasts, and microglia.[19,53] Thus, the use of optimized receptor (and species)-specific small molecular tools is paramount. Selective CB2R activation typically yields immunosuppressive effects, mitigating sterile inflammation and subsequent tissue damage across numerous pathological conditions without exerting psychoactive effects typically associated with CB1R activation. However, it is worth noting that in certain disease contexts/animal models (e.g., where live pathogens are present), CB2R receptor activation might paradoxically exacerbate or instigate tissue injury.[6,54,55] Several puzzling controversies surrounding CB2R biology and expression/target validation may stem from challenges in detecting the CB2R protein (due to the lack of specific antibodies) and the subpar quality of early tool compounds used in preclinical studies, which lacked selectivity, specificity, and had limited bioavailability.[56]

To resolve the apparent contradictions around the therapeutic roles of CB2Rs from mouse models, in addition to conditional tissue-specific knockout mouse lines, selective CB2R receptor ligands with ideal PK properties are essential to determine the physiologically relevant roles of CB2R in health and disease. In a collaborative research effort, we synthesized and profiled a set of highly potent CB2R ligands from literature, including patent literature, here called **RNB** (Roche, NIH and Bern) compounds. **RNB-61** was characterized for the first time in this study. We demonstrate that beyond its remarkable potency and selectivity, **RNB-61** showcases an ideal physicochemical and pharmacokinetic profile. Moreover, its peripherally restricted action enhances its suitability as a premier pharmacological tool for dissecting the pharmaco-

https://doi.org/10.1021/acsptsci.4c00269
ACS Pharmacol. Transl. Sci. 2024, 7, 2424−2438

logical impacts of CB2R across various mammalian cellular systems and animal models.

Selectivity and Potency. Out of the five distinct CB2R agonist evaluated in the current report, **RNB-61** showed the highest (6,800-fold) selectivity toward *h*CB2 against *h*CB1 and showed no significant interaction (defined as >50% inhibition) for 80 additional receptor targets up to 1 μM in a CEREP screen. RNB-61 showed a similar binding affinity for *m*CB2Rs as well as for CB2Rs in different species, indicating that the molecule can be used in preclinical animal models. At 10 μM, which is well above the expected physiological concentration of the compound *in vivo*, the only apparent interaction was with the Na^+ channel. However, given the peripherally restricted action of **RNB-61**, which was confirmed by measuring P-gp interaction, the effect of **RNB-61** on the Na^+ ion channel site 2, which is primarily expressed in neurons of the CNS, is unlikely to translate into marked off-target effects in animal models. Another critical aspect of **RNB-61** for the application in relevant animal models is that in addition to *h*CB2R, the binding affinity of **RNB-61** toward *m*CB2R was similar (EC_{50} < 50 nM). Furthermore, in a functional assay, **RNB-61** also showed comparable potency in four commonly used species for preclinical applications (EC_{50} = 0.13−1.86 nM). Thus, the excellent selectivity profile of **RNB-61** enabled the specific labeling of CB2Rs in membrane preparations from various immune cell lines as well as *ex vivo* tissue slices, which was also supported by the upregulation of CB2R expression upon the LPS-induced inflammatory response in spleen samples of mice.

Physiochemical and Pharmacokinetic Properties. As pointed out by Wu et al.,[12] an optimal balance between selectivity, activity, and pharmacokinetic properties of CB2R ligands needs to be achieved. The pyrazole-derived **RNB- 61** possesses several favorable physiochemical and pharmacokinetic properties. Unlike typical CBR ligands, **RNB-61** has a log*D* value of 3.3, indicating moderate lipophilicity, which accounts for a good balance between solubility and permeability, essential for optimal oral absorption. In accordance, our measurements in four conditions all indicated that **RNB-61** possesses good aqueous solubility (194, 316, 630, and 1373 μg/mL for LYSA, THESA, FaSSiF, and FeSSiF, respectively) that was unexpected due to the high melting point of 188 °C (Table 3). The basic nitrogen atom in the pyrazole ring (N1, basic pK_a: 7.37) likely exerts a positive impact on the solubility, which can be exploited for *in vivo* studies (e.g., i.v. or i.p. administration). In terms of permeability, **RNB-61** crossed cell membranes with a relevant effective permeability of 0.9×10^{-6} cm s^{-1}. In rodent single-dose PK studies, the compound was subject to a low plasma clearance, accounting for ∼5% of hepatic blood flow and in agreement with the intrinsic clearance estimated *in vitro* (Table 3). **RNB-61** displayed an intermediate volume of distribution at a steady state (V_{ss}= 1.6−2.4 L kg^{-1}), suggesting extensive tissue distribution (Figure 4). Taken together, these parameters translated into a terminal plasma half-life of 4−8 h in rats and mice (Table 4).

Peripherally Restricted Action. Different peripherally restricted CB2R agonists have been reported, like the AstraZeneca CB2R ligand, AZD194 or the GlaxoSmithKline's CB2R agonist, GW842166X.[57,58] Despite the low polar surface of 51 $Å^2$ and the presence of only one hydrogen bond donor, **RNB-61** is a strong P-gp substrate in both humans (40.6) and mice (26.8), thus hindering its accumulation in effective concentrations in the CNS. P-gp (also known as multidrug resistance protein 1 (MDR1)) is the most studied and best-characterized drug transporter. Considering the role of CB2R in brain inflammation, a peripherally restricted CB2R full agonist like **RNB-61** may be useful to address the role of CB2R in immune cell infiltration versus microglial activation in the brain. Given the poor selectivity of several CB2R ligands over CB1R, pharmacological experiments addressing the role of CB2Rs in the brain (a topic that is under scientific debate) could potentially be confounded by CB1R agonism. To elucidate the roles of CB2R in neuroinflammatory and neurodegenerative diseases, the coadministration of **RNB-61** and the P-gp inhibitor tariquidar could be performed, mitigating the ambiguities arising from CB1R activity[46] (Table 5).

Nephroprotective Effects. The nephroprotective effects of CB2R signaling have been described using acute kidney injury (AKI), which can often progress to chronic kidney disease (CKD), a debilitating condition affecting more than 10% of the global population. This progressive ailment culminates in kidney fibrosis and failure, presenting significant treatment challenges that remain largely unaddressed. Given the wealth of recent studies highlighting the protective role of CB2R signaling and synthetic agonists in diverse preclinical models of acute and chronic kidney diseases[46,5959], including those induced by the chemotherapy drug cisplatin,[20,21,60] advanced liver injury (hepatorenal syndrome), chronic diabetes,[15,29] I/R,[23,24] and UUO,[25,26] we investigated the efficacy of **RNB-61** in the I/R-induced model of AKI in mice and the UUO-induced kidney fibrosis model in rats. Consistent with previous studies, bilateral kidney I/R injury was associated with significant elevations of serum markers of kidney dysfunction (BUN and creatinine) and parenchymal injury (NGAL, osteopontin, and KIM-1). In the rat model, progressive renal fibrosis developed within 8 days following UUO. **RNB-61** exerted dose-dependent tissue-protective and/or antifibrotic effects in both mice and rats, which were comparable to the effects of the corresponding reference compounds (Fenoldopam, Tempol, Enalapril). Although the evaluation of the expression of CB2R in the kidney injury models and detailed mechanisms of CB2R-mediated nephroprotective effects were beyond the scope of this study, based on a large number of single-cell RNA sequencing databases, it is clear that CB2R is not expressed in cells of normal kidney (neither mouse nor human).[61−72] Under pathological conditions (AKI, fibrosis, diabetes, etc.) CB2R is expressed in various infiltrating immune cells and activated endothelium, but not in parenchyma cells.[69−71] Thus, the protective effects of CB2R agonists observed in our study using models of acute kidney injury and fibrosis are most likely mediated by the attenuation of the inflammatory response and consequent parenchyma injury and fibrogenic response, which is in line with the literature on the protective effect of CB2R in models of tissue injury and fibrosis.

CONCLUSIONS

In summary, our data show that **RNB-61** is a highly potent and bioavailable CB2R-selective full agonist, which serves as the optimal tool compound to investigate the pharmacology of CB2R activation *in vitro* and *in vivo*. Being a substrate for P-gp, RNB-61 can be used either as peripherally restricted CB2R agonist or CNS penetrating CB2R agonist if coadministered with a P-gp inhibitor, allowing the differential investigation of the roles of CB2Rs in the periphery and the CNS, without

https://doi.org/10.1021/acsptsci.4c00269
ACS Pharmacol. Transl. Sci. 2024, 7, 2424−2438

interfering with CB1R activity. In addition, our results support the therapeutic potential of CB2R agonists to treat acute and/or chronic kidney diseases.

■ ASSOCIATED CONTENT

Data Availability Statement

Raw data supporting the conclusions of this article will be made available by the authors upon request.

Supporting Information

The Supporting Information is available free of charge at https://pubs.acs.org/doi/10.1021/acsptsci.4c00269.

CEREP screening for off targets (Figure S1), RNB-61 shows no binding interaction and functional inhibition on endocannabinoid related target proteins (Table S1), synthesis of RNB-61 (Scheme S1), and detailed synthesis procedures (PDF)

■ AUTHOR INFORMATION

Corresponding Authors

Pal Pacher − *Laboratory of Cardiovascular Physiology and Tissue Injury (P.P.), National Institute on Alcohol Abuse and Alcoholism, National Institutes of Health (NIH), Bethesda, MD 20892-9304, United States*; Email: pacher@mail.nih.gov

Jürg Gertsch − *Institute of Biochemistry and Molecular Medicine, University of Bern, Bern 3012, Switzerland*; orcid.org/0000-0003-0978-1555; Email: juerg.gertsch@unibe.ch

Authors

Andrea Chicca − *Institute of Biochemistry and Molecular Medicine, University of Bern, Bern 3012, Switzerland*

Daniel Bátora − *Institute of Biochemistry and Molecular Medicine and Graduate School for Cellular and Biomedical Sciences, University of Bern, Bern 3012, Switzerland*

Christoph Ullmer − *Pharmaceutical Sciences, Roche Innovation Center Basel, Roche Pharma Research and Early Development, Basel 4070, Switzerland*

Antonello Caruso − *Pharmaceutical Sciences, Roche Innovation Center Basel, Roche Pharma Research and Early Development, Basel 4070, Switzerland*; orcid.org/0000-0001-5832-3636

Sabine Grüner − *Pharmaceutical Sciences, Roche Innovation Center Basel, Roche Pharma Research and Early Development, Basel 4070, Switzerland*

Jürgen Fingerle − *Pharmaceutical Sciences, Roche Innovation Center Basel, Roche Pharma Research and Early Development, Basel 4070, Switzerland*

Thomas Hartung − *Pharmaceutical Sciences, Roche Innovation Center Basel, Roche Pharma Research and Early Development, Basel 4070, Switzerland*

Roland Degen − *Pharmaceutical Sciences, Roche Innovation Center Basel, Roche Pharma Research and Early Development, Basel 4070, Switzerland*

Matthias Müller − *Pharmaceutical Sciences, Roche Innovation Center Basel, Roche Pharma Research and Early Development, Basel 4070, Switzerland*

Uwe Grether − *Pharmaceutical Sciences, Roche Innovation Center Basel, Roche Pharma Research and Early Development, Basel 4070, Switzerland*; orcid.org/0000-0002-3164-9270

Complete contact information is available at: https://pubs.acs.org/10.1021/acsptsci.4c00269

Author Contributions

A.Ch. performed conceptualization, investigation, methodology, validation, data curation, and writing − original draft; D.B. was in charge of software, formal analysis, visualization, and writing − original draft; C.U. was in charge of methodology, resource gathering, and writing − original draft; A.Ca. was in charge of methodology and writing − review & editing; J.F. was in charge of methodology, investigation, resource gathering, and writing − review & editing; T.H. was in charge of methodology, supervision, and writing − review & editing; R.D. performed investigation, methodology, and writing − review & editing; M.M. performed investigation, methodology, and writing − review & editing; U.G. performed investigation, methodology, writing − original draft, and supervision; P.P. performed conceptualization, resource gathering, writing − original draft, and supervision; J.G. performed conceptualization, resource gathering, supervision, and writing − original draft, review, and editing.

Funding

JG was supported by the SNFS grant 189220. PP was supported by the Intramural Program of the NIAAA/NIH.

Notes

The authors declare the following competing financial interest(s): Christoph Ullmer, Antonello Caruso, Thomas Hartung, Roland Degen, Matthias Mller, Sabine Grner and Uwe Grether are employees and shareholders of F. Hoffmann-La Roche AG. The remaining authors declare no potential competing interests.

■ ACKNOWLEDGMENTS

The authors wish to thank Camille Perret, Jonathan Mochel, and Franz Schuler for supporting the conduct of the PK and ADME experiments. For the permeability assays, the LLC-PK1 cells were kindly provided by Dr A. Schinkel from The Netherlands Cancer Institute (Amsterdam, The Netherlands)

■ REFERENCES

(1) Zou, S.; Kumar, U. Cannabinoid Receptors and the Endocannabinoid System: Signaling and Function in the Central Nervous System. *Int. J. Mol. Sci.* **2018**, *19* (3), 833. Published Online: 2018. 03. 13.

(2) Maccarrone, M.; Di Marzo, V.; Gertsch, J.; Grether, U.; Howlett, A. C.; Hua, T.; Makriyannis, A.; Piomelli, D.; Ueda, N.; van der Stelt, M. Goods and Bads of the Endocannabinoid System as a Therapeutic Target: Lessons Learned after 30 Years. *Pharmacol. Rev.* **2023**, *75* (5), 885−958. Published Online: 2023. 05. 10.

(3) Bie, B.; Wu, J.; Foss, J. F.; Naguib, M. An overview of the cannabinoid type 2 receptor system and its therapeutic potential. *Current opinion in anaesthesiology* **2018**, *31* (4), 407−414.

(4) Dhopeshwarkar, A.; Mackie, K. CB2 Cannabinoid receptors as a therapeutic target-what does the future hold? *Mol. Pharmacol.* **2014**, *86* (4), 430−437. Published Online: 2014. 08. 08.

(5) Steffens, S.; Pacher, P. Targeting cannabinoid receptor CB(2) in cardiovascular disorders: promises and controversies. *Br. J. Pharmacol.* **2012**, *167* (2), 313−323.

(6) Pacher, P.; Mechoulam, R. Is lipid signaling through cannabinoid 2 receptors part of a protective system? *Progress in lipid research* **2011**, *50* (2), 193−211. Published Online: 2011. 02. 02.

(7) Devane, W. A.; Hanus, L.; Breuer, A.; Pertwee, R. G.; Stevenson, L. A.; Griffin, G.; Gibson, D.; Mandelbaum, A.; Etinger, A.; Mechoulam, R. Isolation and structure of a brain constituent that

binds to the cannabinoid receptor. *Science (New York, N.Y.)* **1992**, *258* (5090), 1946−1949.
(8) Mechoulam, R.; Ben-Shabat, S.; Hanus, L.; Ligumsky, M.; Kaminski, N. E.; Schatz, A. R.; Gopher, A.; Almog, S.; Martin, B. R.; Compton, D. R.; Pertwee, R. G.; Griffin, G.; Bayewitch, M.; Barg, J.; Vogel, Z. Identification of an endogenous 2-monoglyceride, present in canine gut, that binds to cannabinoid receptors. *Biochem. Pharmacol.* **1995**, *50* (1), 83−90.
(9) Banister, S. D.; Connor, M. The Chemistry and Pharmacology of Synthetic Cannabinoid Receptor Agonist New Psychoactive Substances: Evolution. *Handbook of experimental pharmacology* **2018**, *252*, 191−226.
(10) Di Marzo, V. The endocannabinoid system: its general strategy of action, tools for its pharmacological manipulation and potential therapeutic exploitation. *Pharmacological research* **2009**, *60* (2), 77−84. Published Online: 2009. 03. 04.
(11) Gasperi, V.; Guzzo, T.; Topai, A.; Gambacorta, N.; Ciriaco, F.; Nicolotti, O.; Maccarrone, M. Recent Advances on Type-2 Cannabinoid (CB2) Receptor Agonists and their Therapeutic Potential. *Curr. Med. Chem.* **2023**, *30* (12), 1420−1457.
(12) Wu, Y.-R.; Tang, J.-Q.; Zhang, W.-N.; Zhuang, C.-L.; Shi, Y. Rational drug design of CB2 receptor ligands: from 2012 to 2021. *RSC Adv.* **2022**, *12* (54), 35242−35259. Published Online: 2022. 12. 08.
(13) Starowicz, K.; Finn, D. P. Cannabinoids and Pain: Sites and Mechanisms of Action. *Adv. Pharmacol.* **2017**, *80*, 437−475. Published Online: 2017. 06. 20.
(14) Yoo, E. H.; Lee, J. H. Cannabinoids and Their Receptors in Skin Diseases. *International Journal of Molecular Sciences* **2023**, *24* (22), 16523. Published Online: 2023. 11. 20.
(15) Barutta, F.; Piscitelli, F.; Pinach, S.; Bruno, G.; Gambino, R.; Rastaldi, M. P.; Salvidio, G.; Di Marzo, V.; Cavallo Perin, P.; Gruden, G. Protective role of cannabinoid receptor type 2 in a mouse model of diabetic nephropathy. *Diabetes* **2011**, *60* (9), 2386−2396. Published Online: 2011. 08. 01.
(16) Lotersztajn, S.; Teixeira-Clerc, F.; Julien, B.; Deveaux, V.; Ichigotani, Y.; Manin, S.; Tran-Van-Nhieu, J.; Karsak, M.; Zimmer, A.; Mallat, A. CB2 receptors as new therapeutic targets for liver diseases. *Br. J. Pharmacol.* **2008**, *153* (2), 286−289. Published Online: 2007. 10. 22.
(17) Bátkai, S.; Osei-Hyiaman, D.; Pan, H.; El-Assal, O.; Rajesh, M.; Mukhopadhyay, P.; Hong, F.; Harvey-White, J.; Jafri, A.; Haskó, G.; Huffman, J. W.; Gao, B.; Kunos, G.; Pacher, P. Cannabinoid-2 receptor mediates protection against hepatic ischemia/reperfusion injury. *FASEB journal: official publication of the Federation of American Societies for Experimental Biology* **2007**, *21* (8), 1788−1800. Published Online: 2007. 02. 27.
(18) Pacher, P.; Haskó, G. Endocannabinoids and cannabinoid receptors in ischaemia-reperfusion injury and preconditioning. *Br. J. Pharmacol.* **2008**, *153* (2), 252−262. Published Online: 2007. 11. 19.
(19) Gertsch, J. Editorial: Lung macrophages high on cannabinoids: jamming PAMs and taming TAMs? *Journal of leukocyte biology* **2016**, *99* (4), 518−520.
(20) Mukhopadhyay, P.; Baggelaar, M.; Erdelyi, K.; Cao, Z.; Cinar, R.; Fezza, F.; Ignatowska-Janlowska, B.; Wilkerson, J.; van Gils, N.; Hansen, T.; Ruben, M.; Soethoudt, M.; Heitman, L.; Kunos, G.; Maccarrone, M.; Lichtman, A.; Pacher, P.; van der Stelt, M. The novel, orally available and peripherally restricted selective cannabinoid CB2 receptor agonist LEI-101 prevents cisplatin-induced nephrotoxicity. *Br. J. Pharmacol.* **2016**, *173* (3), 446−458. Published Online: 2016. 01. 15.
(21) Mukhopadhyay, P.; Rajesh, M.; Pan, H.; Patel, V.; Mukhopadhyay, B.; Bátkai, S.; Gao, B.; Haskó, G.; Pacher, P. Cannabinoid-2 receptor limits inflammation, oxidative/nitrosative stress, and cell death in nephropathy. *Free radical biology & medicine* **2010**, *48* (3), 457−467. Published Online: 2009. 12. 04.
(22) Trojnar, E.; Erdelyi, K.; Matyas, C.; Zhao, S.; Paloczi, J.; Mukhopadhyay, P.; Varga, Z. V.; Hasko, G.; Pacher, P. Cannabinoid-2 receptor activation ameliorates hepatorenal syndrome. *Free radical biology & medicine* **2020**, *152*, 540−550. Published Online: 2019. 11. 23.
(23) Çakır, M.; Tekin, S.; Doğanyiğit, Z.; Çakan, P.; Kaymak, E. The protective effect of cannabinoid type 2 receptor activation on renal ischemia-reperfusion injury. *Molecular and cellular biochemistry* **2019**, *462* (1−2), 123−132. Published Online: 2019. 08. 24.
(24) Pressly, J. D.; Mustafa, S. M.; Adibi, A. H.; Alghamdi, S.; Pandey, P.; Roy, K. K.; Doerksen, R. J.; Moore, B. M.; Park, F. Selective Cannabinoid 2 Receptor Stimulation Reduces Tubular Epithelial Cell Damage after Renal Ischemia-Reperfusion Injury. *Journal of pharmacology and experimental therapeutics* **2018**, *364* (2), 287−299. Published Online: 2017. 11. 29.
(25) Nettekoven, M.; Adam, J.-M.; Bendels, S.; Bissantz, C.; Fingerle, J.; Grether, U.; Grüner, S.; Guba, W.; Kimbara, A.; Ottaviani, G.; Püllmann, B.; Rogers-Evans, M.; Röver, S.; Rothenhäusler, B.; Schmitt, S.; Schuler, F.; Schulz-Gasch, T.; Ullmer, C. Novel Triazolopyrimidine-Derived Cannabinoid Receptor 2 Agonists as Potential Treatment for Inflammatory Kidney Diseases. *ChemMedChem.* **2016**, *11* (2), 179−189. Published Online: 2015. 07. 21.
(26) Swanson, M. L.; Regner, K. R.; Moore, B. M.; Park, F. Cannabinoid Type 2 Receptor Activation Reduces the Progression of Kidney Fibrosis Using a Mouse Model of Unilateral Ureteral Obstruction. *Cannabis and cannabinoid research* **2022**, *7* (6), 790−803. Published Online: 2022. 02. 23.
(27) Hickey, E. R.; Zindell, R.; Cirillo, P. F.; Wu, L.; Ermann, M.; Berry, A. K.; Thomson, D. S.; Albrecht, C.; Gemkow, M. J.; Riether, D. Selective CB2 receptor agonists. Part 1: the identification of novel ligands through computer-aided drug design (CADD) approaches. *Bioorganic & medicinal chemistry letters* **2015**, *25* (3), 575−580. Published Online: 2014. 12. 17.
(28) Long, C.; Xie, N.; Shu, Y.; Wu, Y.; He, P.; Zhou, Y.; Xiang, Y.; Gu, J.; Yang, L.; Wang, Y. Knockout of the Cannabinoid Receptor 2 Gene Promotes Inflammation and Hepatic Stellate Cell Activation by Promoting A20/Nuclear Factor-κB (NF-κB) Expression in Mice with Carbon Tetrachloride-Induced Liver Fibrosis. *Med. Sci. Monit.* **2021**, *27*, No. e931236-1. Published Online: 2021. 08. 20.
(29) Barutta, F.; Grimaldi, S.; Franco, I.; Bellini, S.; Gambino, R.; Pinach, S.; Corbelli, A.; Bruno, G.; Rastaldi, M. P.; Aveta, T.; Hirsch, E.; Di Marzo, V.; Gruden, G. Deficiency of cannabinoid receptor of type 2 worsens renal functional and structural abnormalities in streptozotocin-induced diabetic mice. *Kidney international* **2014**, *86* (5), 979−990. Published Online: 2014. 05. 14.
(30) Soethoudt, M.; Grether, U.; Fingerle, J.; Grim, T. W.; Fezza, F.; de Petrocellis, L.; Ullmer, C.; Rothenhäusler, B.; Perret, C.; van Gils, N.; Finlay, D.; MacDonald, C.; Chicca, A.; Gens, M. D.; Stuart, J.; de Vries, H.; Mastrangelo, N.; Xia, L.; Alachouzos, G.; Baggelaar, M. P.; Martella, A.; Mock, E. D.; Deng, H.; Heitman, L. H.; Connor, M.; Di Marzo, V.; Gertsch, J.; Lichtman, A. H.; Maccarrone, M.; Pacher, P.; Glass, M.; van der Stelt, M. Cannabinoid CB2 receptor ligand profiling reveals biased signalling and off-target activity. *Nat. Commun.* **2017**, *8* (1), 13958. Published Online: 2017. 01. 03.
(31) Yao, B. B.; Hsieh, G. C.; Frost, J. M.; Fan, Y.; Garrison, T. R.; Daza, A. V.; Grayson, G. K.; Zhu, C. Z.; Pai, M.; Chandran, P.; Salyers, A. K.; Wensink, E. J.; Honore, P.; Sullivan, J. P.; Dart, M. J.; Meyer, M. D. In vitro and in vivo characterization of A-796260: a selective cannabinoid CB2 receptor agonist exhibiting analgesic activity in rodent pain models. *Br. J. Pharmacol.* **2008**, *153* (2), 390−401. Published Online: 2007. 11. 12.
(32) Carroll, W. A.; Dart, M. J.; Frost, J. M.; Latshaw, S. P.; Kolasa, T.; Li, T.; Peddi, S.; Liu, B.; Peddi, S.; Liu, B.; Perez-Medrano, A.; Patel, M.; Wang, X.; Nelson, D. W. Novel compounds as cannabinoid receptor ligands. 12/560,893.
(33) Cheng, Y.; Albrecht, B. K.; Brown, J.; Buchanan, J. L.; Buckner, W. H.; DiMauro, E. F.; Emkey, R.; Fremeau, R. T.; Harmange, J.-C.; Hoffman, B. J.; Huang, L.; Huang, M.; Lee, J. H.; Lin, F.-F.; Martin, M. W.; Nguyen, H. Q.; Patel, V. F.; Tomlinson, S. A.; White, R. D.; Xia, X.; Hitchcock, S. A. Discovery and optimization of a novel series of N-arylamide oxadiazoles as potent, highly selective and orally bioavailable cannabinoid receptor 2 (CB2) agonists. *Journal of*

https://doi.org/10.1021/acsptsci.4c00269
ACS Pharmacol. Transl. Sci. 2024, 7, 2424−2438

medicinal chemistry **2008**, *51* (16), 5019−5034. Published Online: 2008. 08. 05.
(34) Cirillo, P. F.; Hickey, E. R.; Riether, D.; Ermann, M.; Mushi, I. Amine and ether compounds which modulate the cb2 receptor. U.S. Patent 8,957,063.
(35) Bartolozzi, A.; Hickey, E. R.; Riether, D.; Wu, L.; Zindell, R. M.; East, S. P., Monika Ermann. Compounds Which Selectively Modulate The CB2 Receptor.
(36) Chicca, A.; Nicolussi, S.; Bartholomäus, R.; Blunder, M.; Aparisi Rey, A.; Petrucci, V.; del Carmen Reynoso-Moreno, I.; Viveros-Paredes, J. M.; Dalghi Gens, M.; Lutz, B.; Schiöth, H. B.; Soeberdt, M.; Abels, C.; Charles, R. P.; Altmann, K. H.; Gertsch, J. Chemical probes to potently and selectively inhibit endocannabinoid cellular reuptake. *Proc. Natl. Acad. Sci. U.S.A.* **2017**, *114* (25), E5006−E5015.
(37) Porter, R. F.; Szczesniak, A. M.; Toguri, J. T.; Gebremeskel, S.; Johnston, B.; Lehmann, C.; Fingerle, J.; Rothenhäusler, B.; Perret, C.; Rogers-Evans, M.; Kimbara, A.; Nettekoven, M.; Guba, W.; Grether, U.; Ullmer, C.; Kelly, M. E. M. Selective Cannabinoid 2 Receptor Agonists as Potential Therapeutic Drugs for the Treatment of Endotoxin-Induced Uveitis. *Molecules (Basel, Switzerland)* **2019**, *24* (18). DOI: 3338. Published Online: 2019. 09. 13.
(38) Wagner, B.; Fischer, H.; Kansy, M.; Seelig, A.; Assmus, F. Carrier Mediated Distribution System (CAMDIS): a new approach for the measurement of octanol/water distribution coefficients. *European journal of pharmaceutical sciences: official journal of the European Federation for Pharmaceutical Sciences* **2015**, *68*, 68−77. Published Online: 2014. 12. 13.
(39) Mock, E. D.; Mustafa, M.; Gunduz-Cinar, O.; Cinar, R.; Petrie, G. N.; Kantae, V.; Di, X.; Ogasawara, D.; Varga, Z. V.; Paloczi, J.; Miliano, C.; Donvito, G.; van Esbroeck, A. C. M.; van der Gracht, A. M. F.; Kotsogianni, I.; Park, J. K.; Martella, A.; van der Wel, T.; Soethoudt, M.; Jiang, M.; Wendel, T. J.; Janssen, A. P. A.; Bakker, A. T.; Donovan, C. M.; Castillo, L. I.; Florea, B. I.; Wat, J.; van den Hurk, H.; Wittwer, M.; Grether, U.; Holmes, A.; van Boeckel, C. A. A.; Hankemeier, T.; Cravatt, B. F.; Buczynski, M. W.; Hill, M. N.; Pacher, P.; Lichtman, A. H.; van der Stelt, M. Discovery of a NAPE-PLD inhibitor that modulates emotional behavior in mice. *Nat. Chem. Biol.* **2020**, *16* (6), 667−675. Published Online: 2020. 05. 11.
(40) He, Y.; Schild, M.; Grether, U.; Benz, J.; Leibrock, L.; Heer, D.; Topp, A.; Collin, L.; Kuhn, B.; Wittwer, M.; Keller, C.; Gobbi, L. C.; Schibli, R.; Mu, L. Development of High Brain-Penetrant and Reversible Monoacylglycerol Lipase PET Tracers for Neuroimaging. *Journal of medicinal chemistry* **2022**, *65* (3), 2191−2207. Published Online: 2022. 01. 28.
(41) Fowler, S.; Zhang, H. In vitro evaluation of reversible and irreversible cytochrome P450 inhibition: current status on methodologies and their utility for predicting drug-drug interactions. *AAPS journal* **2008**, *10* (2), 410−424. Published Online: 2008. 08. 07.
(42) Brink, A.; Fontaine, F.; Marschmann, M.; Steinhuber, B.; Cece, E. N.; Zamora, I.; Pähler, A. Post-acquisition analysis of untargeted accurate mass quadrupole time-of-flight MS(E) data for multiple collision-induced neutral losses and fragment ions of glutathione conjugates. *Rapid communications in mass spectrometry: RCM* **2014**, *28* (24), 2695−2703.
(43) Zhang, W.; Guo, L.; Liu, H.; Wu, G.; Shi, H.; Zhou, M.; Zhang, Z.; Kou, B.; Hu, T.; Zhou, Z.; Xu, Z.; Zhou, X.; Zhou, Y.; Tian, X.; Yang, G.; Young, J. A. T.; Qiu, H.; Ottaviani, G.; Xie, J.; Mayweg, A. V.; Shen, H. C.; Zhu, W. Discovery of Linvencorvir (RG7907), a Hepatitis B Virus Core Protein Allosteric Modulator, for the Treatment of Chronic HBV Infection. *Journal of medicinal chemistry* **2023**, *66* (6), 4253−4270. Published Online: 2023. 03. 10.
(44) Haider, A.; Gobbi, L.; Kretz, J.; Ullmer, C.; Brink, A.; Honer, M.; Woltering, T. J.; Muri, D.; Iding, H.; Bürkler, M.; Binder, M.; Bartelmus, C.; Knuesel, I.; Pacher, P.; Herde, A. M.; Spinelli, F.; Ahmed, H.; Atz, K.; Keller, C.; Weber, M.; Schibli, R.; Mu, L.; Grether, U.; Ametamey, S. M. Identification and Preclinical Development of a 2,5,6-Trisubstituted Fluorinated Pyridine Derivative as a Radioligand for the Positron Emission Tomography Imaging of Cannabinoid Type 2 Receptors. *Journal of medicinal chemistry* **2020**, *63* (18), 10287−10306. Published Online: 2020. 09. 01.
(45) Poirier, A.; Cascais, A.-C.; Bader, U.; Portmann, R.; Brun, M.-E.; Walter, I.; Hillebrecht, A.; Ullah, M.; Funk, C. Calibration of in vitro multidrug resistance protein 1 substrate and inhibition assays as a basis to support the prediction of clinically relevant interactions in vivo. *Drug metabolism and disposition: the biological fate of chemicals* **2014**, *42* (9), 1411−1422. Published Online: 2014. 06. 17.
(46) Fox, E.; Bates, S. E. Tariquidar (XR9576): a P-glycoprotein drug efflux pump inhibitor. *Expert review of anticancer therapy* **2007**, *7* (4), 447−459.
(47) Skrypnyk, N. I.; Harris, R. C.; de Caestecker, M. P. Ischemia-reperfusion model of acute kidney injury and post injury fibrosis in mice. *JoVE* **2013**, No. 78, No. e50495.
(48) Feizi, A.; Jafari, M.-R.; Hamedivafa, F.; Tabrizian, P.; Djahanguiri, B. The preventive effect of cannabinoids on reperfusion-induced ischemia of mouse kidney. *Experimental and toxicologic pathology: official journal of the Gesellschaft fur Toxikologische Pathologie* **2008**, *60* (4−5), 405−410. Published Online: 2008. 06. 20.
(49) Chevalier, R. L.; Forbes, M. S.; Thornhill, B. A. Ureteral obstruction as a model of renal interstitial fibrosis and obstructive nephropathy. *Kidney international* **2009**, *75* (11), 1145−1152. Published Online: 2009. 04. 01.
(50) Noce, A.; Marrone, G.; Rovella, V.; Busca, A.; Gola, C.; Ferrannini, M.; Di Daniele, N. Fenoldopam Mesylate: A Narrative Review of Its Use in Acute Kidney Injury. *Current pharmaceutical biotechnology* **2019**, *20* (5), 366−375.
(51) Atwood, B. K.; Straiker, A.; Mackie, K. CB_2: therapeutic target-in-waiting. *Progress in neuro-psychopharmacology & biological psychiatry* **2012**, *38* (1), 16−20. Published Online: 2011. 12. 09.
(52) Cabañero, D.; Martín-García, E.; Maldonado, R. The CB2 cannabinoid receptor as a therapeutic target in the central nervous system. *Expert opinion on therapeutic targets* **2021**, *25* (8), 659−676. Published Online: 2021. 09. 23.
(53) Horváth, B.; Magid, L.; Mukhopadhyay, P.; Bátkai, S.; Rajesh, M.; Park, O.; Tanchian, G.; Gao, R. Y.; Goodfellow, C. E.; Glass, M.; Mechoulam, R.; Pacher, P. A new cannabinoid CB2 receptor agonist HU-910 attenuates oxidative stress, inflammation and cell death associated with hepatic ischaemia/reperfusion injury. *Br. J. Pharmacol.* **2012**, *165* (8), 2462−2478.
(54) Alferink, J.; Specht, S.; Arends, H.; Schumak, B.; Schmidt, K.; Ruland, C.; Lundt, R.; Kemter, A.; Dlugos, A.; Kuepper, J. M.; Poppensieker, K.; Findeiss, M.; Albayram, Ö.; Otte, D.-M.; Marazzi, J.; Gertsch, J.; Förster, I.; Maier, W.; Scheu, S.; Hoerauf, A.; Zimmer, A. Cannabinoid Receptor 2 Modulates Susceptibility to Experimental Cerebral Malaria through a CCL17-dependent Mechanism. *J. Biol. Chem.* **2016**, *291* (37), 19517−19531. Published Online: 2016. 07. 29.
(55) Maccarrone, M.; Bab, I.; Bíró, T.; Cabral, G. A.; Dey, S. K.; Di Marzo, V.; Konje, J. C.; Kunos, G.; Mechoulam, R.; Pacher, P.; Sharkey, K. A.; Zimmer, A. Endocannabinoid signaling at the periphery: 50 years after THC. *Trends in pharmacological sciences* **2015**, *36* (5), 277−296. Published Online: 2015. 03. 18.
(56) Uwe Grether, P. P. Challenges bringing CB_2R medicine to bedside. *Open Access Government*, **2023**. 01. 03. https://www.openaccessgovernment.org/article/challenges-bringing-cb%E2%82%82r-medicine-to-bedside/150463/ (accessed 2024. 04. 25.).
(57) Naguib, M.; Diaz, P.; Xu, J. J.; Astruc-Diaz, F.; Craig, S.; Vivas-Mejia, P.; Brown, D. L. MDA7: a novel selective agonist for CB2 receptors that prevents allodynia in rat neuropathic pain models. *Br. J. Pharmacol.* **2008**, *155* (7), 1104−1116. Published Online: 2008. 09. 01.
(58) Battista, N.; Di Tommaso, M.; Bari, M.; Maccarrone, M. The endocannabinoid system: an overview. *Frontiers in Behavioral Neuroscience* **2012**, *6*, 9. Published Online: 2012. 03. 14.
(59) Zhao, Z.; Yan, Q.; Xie, J.; Liu, Z.; Liu, F.; Liu, Y.; Zhou, S.; Pan, S.; Liu, D.; Duan, J.; Liu, Z. The intervention of cannabinoid receptor

in chronic and acute kidney disease animal models: a systematic review and meta-analysis. *Diabetology & metabolic syndrome* **2024**, *16* (1), 45. Published Online: 2024. 02. 15.
(60) Li, X.; Chang, H.; Bouma, J.; de Paus, L. V.; Mukhopadhyay, P.; Paloczi, J.; Mustafa, M.; van der Horst, C.; Kumar, S. S.; Wu, L.; Yu, Y.; van den Berg, R. J. B. H. N.; Janssen, A. P. A.; Lichtman, A.; Liu, Z.-J.; Pacher, P.; van der Stelt, M.; Heitman, L. H.; Hua, T. Structural basis of selective cannabinoid CB2 receptor activation. *Nat. Commun.* **2023**, *14* (1), 1447. Published Online: 2023. 03. 15.
(61) Wu, H.; Gonzalez Villalobos, R.; Yao, X.; Reilly, D.; Chen, T.; Rankin, M.; Myshkin, E.; Breyer, M. D.; Humphreys, B. D. Mapping the single-cell transcriptomic response of murine diabetic kidney disease to therapies. *Cell Metab.* **2022**, *34* (7), 1064−1078.e6. Published Online: 2022. 06. 15.
(62) Ferreira, R. M.; Sabo, A. R.; Winfree, S.; Collins, K. S.; Janosevic, D.; Gulbronson, C. J.; Cheng, Y. H.; Casbon, L.; Barwinska, D.; Ferkowicz, M. J.; Xuei, X.; Zhang, C.; Dunn, K. W.; Kelly, K. J.; Sutton, T. A.; Hato, T.; Dagher, P. C.; El-Achkar, T. M.; Eadon, M. T. Integration of spatial and single-cell transcriptomics localizes epithelial cell-immune cross-talk in kidney injury. *JCI insight* **2021**, *6* (12), No. e147703.
(63) Li, H.; Dixon, E. E.; Wu, H.; Humphreys, B. D. Comprehensive single-cell transcriptional profiling defines shared and unique epithelial injury responses during kidney fibrosis. *Cell Metab.* **2022**, *34* (12), 1977−1998.e9. Published Online: 2022. 10. 19.
(64) Gerhardt, L. M. S.; Koppitch, K.; van Gestel, J.; Guo, J.; Cho, S.; Wu, H.; Kirita, Y.; Humphreys, B. D.; McMahon, A. P. Lineage Tracing and Single-Nucleus Multiomics Reveal Novel Features of Adaptive and Maladaptive Repair after Acute Kidney Injury. *Journal of the American Society of Nephrology: JASN* **2023**, *34* (4), 554−571. Published Online: 2023. 01. 13.
(65) Balzer, M. S.; Doke, T.; Yang, Y.-W.; Aldridge, D. L.; Hu, H.; Mai, H.; Mukhi, D.; Ma, Z.; Shrestha, R.; Palmer, M. B.; Hunter, C. A.; Susztak, K. Single-cell analysis highlights differences in druggable pathways underlying adaptive or fibrotic kidney regeneration. *Nat. Commun.* **2022**, *13* (1), 4018. Published Online: 2022. 07. 11.
(66) Wu, H.; Kirita, Y.; Donnelly, E. L.; Humphreys, B. D. Advantages of Single-Nucleus over Single-Cell RNA Sequencing of Adult Kidney: Rare Cell Types and Novel Cell States Revealed in Fibrosis. *Journal of the American Society of Nephrology: JASN* **2019**, *30* (1), 23−32. Published Online: 2018. 12. 03.
(67) Wilson, P. C.; Muto, Y.; Wu, H.; Karihaloo, A.; Waikar, S. S.; Humphreys, B. D. Multimodal single cell sequencing implicates chromatin accessibility and genetic background in diabetic kidney disease progression. *Nat. Commun.* **2022**, *13* (1), 5253. Published Online: 2022. 09. 06.
(68) Muto, Y.; Dixon, E. E.; Yoshimura, Y.; Wu, H.; Omachi, K.; Ledru, N.; Wilson, P. C.; King, A. J.; Eric Olson, N.; Gunawan, M. G.; Kuo, J. J.; Cox, J. H.; Miner, J. H.; Seliger, S. L.; Woodward, O. M.; Welling, P. A.; Watnick, T. J.; Humphreys, B. D. Defining cellular complexity in human autosomal dominant polycystic kidney disease by multimodal single cell analysis. *Nat. Commun.* **2022**, *13* (1), 6497. Published Online: 2022. 10. 30.
(69) Wu, H.; Malone, A. F.; Donnelly, E. L.; Kirita, Y.; Uchimura, K.; Ramakrishnan, S. M.; Gaut, J. P.; Humphreys, B. D. Single-Cell Transcriptomics of a Human Kidney Allograft Biopsy Specimen Defines a Diverse Inflammatory Response. *Journal of the American Society of Nephrology: JASN* **2018**, *29* (8), 2069−2080. Published Online: 2018. 07. 06.
(70) Wu, H.; Uchimura, K.; Donnelly, E. L.; Kirita, Y.; Morris, S. A.; Humphreys, B. D. Comparative Analysis and Refinement of Human PSC-Derived Kidney Organoid Differentiation with Single-Cell Transcriptomics. *Cell Stem Cell* **2018**, *23* (6), 869−881.e8. Published Online: 2018. 11. 15.
(71) Wilson, P. C.; Wu, H.; Kirita, Y.; Uchimura, K.; Ledru, N.; Rennke, H. G.; Welling, P. A.; Waikar, S. S.; Humphreys, B. D. The single-cell transcriptomic landscape of early human diabetic nephropathy. *Proc. Natl. Acad. Sci. U.S.A.* **2019**, *116* (39), 19619−19625. Published Online: 2019. 09. 10.
(72) Muto, Y.; Wilson, P. C.; Ledru, N.; Wu, H.; Dimke, H.; Waikar, S. S.; Humphreys, B. D. Single cell transcriptional and chromatin accessibility profiling redefine cellular heterogeneity in the adult human kidney. *Nat. Commun.* **2021**, *12* (1), 2190. Published Online: 2021. 04. 13.

https://doi.org/10.1021/acsptsci.4c00269
ACS Pharmacol. Transl. Sci. 2024, 7, 2424−2438